Journal of Photochemistry & Photobiology, A: Chemistry 435 (2023) 114290

Contents lists available at ScienceDirect

Journal of Photochemistry & Photobiology, A: Chemistry

journal homepage: www.elsevier.com/locate/jphotochem

Titanium dioxide nanoparticle-based hydroxyl and superoxide radical production for oxidative stress biological simulations

Marianna Skipitari [a,1], Electra Kalaitzopoulou [a,1], Polyxeni Papadea [a], Athina Varemmenou [b], Vassilios E. Gavriil [c], Evangelia Sarantopoulou [c], Alkiviadis-Constantinos Cefalas [c], Sotiris Tsakas [a], Eleftheria Rosmaraki [a], Irene Margiolaki [a], Tilman Grune [d,e], Christos D. Georgiou [a,*]

[a] Section of Genetics, Cell Biology and Development, Department of Biology, University of Patras, Patras 26504, Greece
[b] Department of Medicine, University of Patras, Patras 26504, Greece
[c] Theoretical and Physical Chemistry Institute, National Hellenic Research Foundation, Athens 11635, Greece
[d] Department of Molecular Toxicology, German Institute of Human Nutrition, Potsdam-Rehbrücke, Germany
[e] Department of Physiological Chemistry, Faculty of Chemistry, University of Vienna, Vienna, Austria

ARTICLE INFO

Keywords:
Titanium dioxide nanoparticles
Superoxide radical
Hydroxyl radical
Oxidative stress
Fenton reaction

ABSTRACT

The present study introduces a TiO_2 nanoparticle-based ($TiO_{2\text{-NP}}$) system for the generation of $^{\bullet}OH$ and $O_2^{\bullet-}$ upon visible photo-excitation, in order to be used for high oxidative stress biological simulations *in vitro*. The main novelties of $TiO_{2\text{-NP}}$ system are: It is set to produce $^{\bullet}OH$ and $O_2^{\bullet-}$ alone or both (in contrast to $^{\bullet}OH$-based common use of TiO_2), as these options cover all possible generation means of these radicals in biological systems *in vivo*. Moreover, the known non-specific electrostatic interactions of $TiO_{2\text{-NP}}$ with H_2O and various biological systems (e.g., cells, membrane proteins, even drugs) simulate direct/distant interactions of any *in vivo* $^{\bullet}OH$, $O_2^{\bullet-}$ source with extra/intracellular biological targets taking place in a densely packed biomolecular environment. The $TiO_{2\text{-NP}}$ system can use any commercially available $TiO_{2\text{-NP}}$ source (dispersion, nanopowder, crystal type), as long as $TiO_{2\text{-NPs}}$' concentrations in use meet the critical criterion to produce $^{\bullet}OH$ levels linearly proportional to irradiation time, set for a given simulation study. The $TiO_{2\text{-NP}}$ system is calibrated by a standardized protocol developed to be applicable to most biological systems, offering the option of $TiO_{2\text{-NP}}$ removal via coagulation when needed. The production rates of $^{\bullet}OH$ and $O_2^{\bullet-}$ by the $TiO_{2\text{-NP}}$ system are specifically calibrated with the respective specific probes terephthalic acid (TPA) and hydroethidine (HE), and tested in comparison to the $^{\bullet}OH$-producing Fenton system. The reaction kinetics of $^{\bullet}OH$ and $O_2^{\bullet-}$ with TPA and HE is found to be in competition with their generating source, the $TiO_{2\text{-NP}}$ system. Similar ROS source competition phenomena with biological targets (simulated by TPA/HE) are very common in biological systems. In contrast, the Fenton system is shown not to exhibit such competition kinetics. The $TiO_{2\text{-NP}}$ system can be used to study $^{\bullet}OH/O_2^{\bullet-}$ dose–response-depended oxidative modifications in biological simulations. This stems from the fact that $^{\bullet}OH$ and $O_2^{\bullet-}$ linear production rates (60 min and up to 8 min, respectively) can be controlled by varying (i) TiO_2 concentration, (ii) light-source photon emission energy (decreasing from 370 to 410 nm), and (iii) light intensity (as a function of the inverse of squared distance from the irradiated sample). In contrast, $^{\bullet}OH$ production by the Fenton system reaches steady state in ~5 s regardless of varying Fe-II concentration, rendering it inappropriate for $^{\bullet}OH$ simulation studies on biological systems. The biological simulating potential of the $TiO_{2\text{-NP}}$ system, as producer of both $^{\bullet}OH$ and $O_2^{\bullet-}$, is also experimentally verified on indicative biological examples selected to structurally represent most biological systems: BSA, a model hydrophilic protein; LDL, structurally resembling most of the biological systems (cells, membranes, organelles, lipoproteins, proteins, lipids). The $TiO_{2\text{-NP}}$ system causes a linear increase of all the tested oxidative modifications on both BSA and LDL for irradiation exposure 20 to 40 min, which strongly suggests that they are mainly $^{\bullet}OH$ dose-proportional. In contrast, the Fenton system does not display $^{\bullet}OH$ dose-associated oxidative modifications on BSA.

* Corresponding author.
E-mail address: c.georgiou@upatras.gr (C.D. Georgiou).
[1] M.S and E.K. have equal contribution.

https://doi.org/10.1016/j.jphotochem.2022.114290
Received 6 July 2022; Received in revised form 2 September 2022; Accepted 17 September 2022
Available online 21 September 2022

1. Introduction

The major reactive oxygen species (ROS), formed continuously in organisms are the hydroxyl ($^{\bullet}OH$) and superoxide ($O_2^{\bullet-}$) radicals, with their many roles, formation, lifetimes, and reactions having been very early realized [1,2]. Among the two, $^{\bullet}OH$ is linked to several diseases such as aging, brain ischemia, carcinogenesis, cardiovascular and neurodegenerating diseases [3], as being the most reactive (with DNA, proteins, lipids etc.). Although less drastic, $O_2^{\bullet-}$ has been associated with similar biological effects, mainly through its dismutation product H_2O_2 conversion to $^{\bullet}OH$ by biologically important reduced transition metals [3,4].

$^{\bullet}OH$ and $O_2^{\bullet-}$ generation takes place in cells (eukaryotic/microbial) or even in biological fluids such as blood serum, almost in contact with its biological molecular targets, which is displayed also by their short half-life, and the locations of their generation sources and molecular targets. $^{\bullet}OH$ half-life is very short (10^{-9} s) [2,5], a reflection of its very low *in vivo* steady state concentration as being the most reactive among oxygen free radicals due to its comparatively high reduction potential [6]. In contrast, $O_2^{\bullet-}$ half-life is ~5 s at physiological pH [7], and its steady-state concentrations are in the range of 10^{-11} to 10^{-12} mol L^{-1} due to the high intracellular activities of superoxide dimutase (SOD) [8]; SOD converts $O_2^{\bullet-}$ to H_2O_2 (and gaseous O_2).

In terms of generation sources/mechanisms, $O_2^{\bullet-}$ is mainly produced in the inner mitochondrial membrane, besides being produced also by cellular reductants [9]. Indicatively, $O_2^{\bullet-}$ inactivates iron-sulfur-containing (de)hydratases (e.g., the intra-mitochondrial Krebs cycle aconitase) by release of the Fe atom and oxidation of the $[4Fe\text{-}4S]^{2+}$ cluster [9,10] while reduces free Fe^{3+} [11,12], which can then react with target-adjacent H_2O_2 and other organic (lipid) hydroperoxides to generate $^{\bullet}OH$ and other alkoxyl radicals [10] by Fenton reaction [13]. Therefore, $^{\bullet}OH$ are formed non-enzymatically by the Fenton reaction, and to a lesser degree by cell-wall peroxidases in the presence, *in vivo*, of O_2 and NADH [14].

In terms of molecular targets for $^{\bullet}OH$ and $O_2^{\bullet-}$, these compete with numerous primary or secondary molecular targets, which form a densely packed intracellular molecular environment. Proteins are a typical example of closely adjacent and competing multitarget example, since they constitute the highest cell dry weight (~55 %; RNA ~20 %, lipids ~10 %, DNA ~3 %, the rest from polysaccharides, metabolites, ions etc.) [15], an idea of them being of the most adjacent targets of $^{\bullet}OH$ and $O_2^{\bullet-}$, is given by their very dense packing inside a cell volume. They occupy 15–35 % [16] of the ~4000 μm^3 cell volume [17], which corresponds to 2–4 million proteins per μm^3 [18]. Even in biological fluids such as blood serum, albumins (e.g., bovine serum albumin; BSA) exist at very high concentrations (~35 to 55 mg/mL [19,20]). Adding to that, is the dynamic nature of this dense packing if these 3D shapes of proteins are viewed also under an intricate interplay with cytoskeletal microfilaments of actin, microtubules, myosin, and kinesin [21]. Surface associated cellular interactions, interconnected with the dense cytoskeleton, are most pronounced on protein surface [22], protein-lipid [23] and protein-protein interactions [24]. Moreover, the ~70 % water content in cells exists not as individual H_2O molecules randomly moving around but making clusters (held together mostly by H-bonds), which can reach molecular mass >20 kDa, and form solid-like phases with the microfilament cytoskeleton network [25].

Given the extremely transient appearance of $^{\bullet}OH$ and $O_2^{\bullet-}$ in all aerobic biological systems their oxidative effects *in vivo* are experimentally infeasible to follow at present, and it has been addressed with biological simulation experiments using artificial generators of $^{\bullet}OH$ and $O_2^{\bullet-}$ (to a lesser degree). Traditionally, the employed artificial systems for oxidative stress (OS) simulation studies are based on $^{\bullet}OH$ generation by the standard Fenton reaction (Eq. (1)) [13], which besides $^{\bullet}OH$ exposes the biological systems to H_2O_2. However, investigations on its reaction mechanism have uncovered the following additional side reactions [26–28], where the Fe^{2+} reactant is oxidized/regenerated (Eqs. (2) to (5)) or $O_2^{\bullet-}$ is generated (Eqs. (2) and (6)):

$$Fe^{2+} + H_2O_2 \rightarrow Fe^{3+} + OH^- + {}^{\cdot}OH \quad (1)$$

$$Fe^{2+} + O_2 \leftrightarrow Fe^{3+} + O_2^{\cdot-} \quad (2)$$

$$Fe^{2+} + {}^{\cdot}OH \rightarrow Fe^{3+} + HO^- \quad (3)$$

$$Fe^{2+} + HO_2^{\cdot} \rightarrow Fe^{3+} + HO_2^- \quad (4)$$

$$Fe^{3+} + HO_2^{\cdot} \rightarrow Fe^{2+} + H^+ + O_2 \quad (5)$$

$$Fe^{3+} + H_2O_2 \rightarrow Fe^{2+} + H^+ + HO_2^{\cdot} \quad (6)$$

Additional complications arise from variations of the standard Fenton system, involving Fe^{2+} regeneration via Fe^{3+} reduction by ascorbic acid (Asc) [29]. Moreover, Asc besides its antioxidant interference is involved in $^{\bullet}OH$ production as well, deriving from the oxidation of ascorbate monoanion ($AscH^-$) by the Fenton reagent H_2O_2 [30]:

$$AscH^- + H_2O_2 \rightarrow Asc^{\cdot-} + H_2O + {}^{\cdot}OH \quad (7)$$

Equally important complication is the fact that $^{\bullet}OH$ production by the Fenton reaction (Eq. (1)) is very fast (~30 s, regardless of Fe^{2+} concentration), due to its relatively fast rate constant 230 $M^{-1}s^{-1}$ [31]. Besides the Fenton reaction itself which also takes place in biological systems [32], the rest of the above reasons render the standard Fenton system not specific for $^{\bullet}OH$ (it involves H_2O_2 and produces $O_2^{\bullet-}$), and its variations (using antioxidant Asc) inappropriate for high OS biological simulation studies.

In reference to the $O_2^{\bullet-}$ production systems (by the xanthine/xanthine oxidase (XO) system [33], NADPH-phenazine methosulfate (PMS) system [34], and the auto-oxidation of pyrogallol [35]), their use in biological systems has been very limited [36–38], mainly due to uncontrolled $O_2^{\bullet-}$ rates and oxidative side reaction products, which render these systems inappropriate for studies simulating $O_2^{\bullet-}$ interactions with biological systems. More specifically, the enzymic XO system produces as its main product the oxidant H_2O_2, while $O_2^{\bullet-}$ is produced even up to 3-fold less, [39]. Another disadvantage of the XO-system is the requirement of pure O_2 constant bubbling, while counting as advantage its proteinic nature for biological simulation studies. Similarly, the NADPH-PMS system does not have $O_2^{\bullet-}$ as its main product, as being a side product of PMS auto-oxidation, while it also requires a constant supply of O_2. Considering the system that is based on the auto-oxidation of pyrogallol for $O_2^{\bullet-}$ production, besides taking place at alkaline pH under O_2 supply, the system also produces a highly reactive semiquinone free radical product [35].

In light of the limitations of the aforementioned artificial generators of $^{\bullet}OH$ and $O_2^{\bullet-}$ as high OS simulators of a densely packed intra/extracellular molecular environment, the present study investigates for the first time the development of a TiO_2 nanoparticle ($TiO_{2\text{-}NP}$) $^{\bullet}OH/O_2^{\bullet-}$ generation system. The $TiO_{2\text{-}NP}$ system is a more appropriate high OS simulant because of the following considerations, which make it innovative: **1.** $TiO_{2\text{-}NP}$ have been modeled to directly interact with H_2O by forming a surface monolayer, where the most pronounced H_2O dipole orientation effects are exerted, which is further extended to a 0.5-nm-thick spherical shell [40]. **2.** $TiO_{2\text{-}NP}$ is appropriate for *in vitro* interactions with various biological systems since it has been shown to exhibit non-specific electrostatic interactions with various biological systems, e.g., with cells [41], cell membrane proteins [42], organic molecules (such as drugs [43]; however, such interactions render $TiO_{2\text{-}NP}$ inappropriate for *in vivo* studies with multicellular organisms or cell cultures during growth. **3.** Another advantage of our $TiO_{2\text{-}NP}$ system stems from the fact that we use for its development a commercial $TiO_{2\text{-}NP}$ mixture of anatase-rutile. The reason being, there are important differences in $^{\bullet}OH$ formation between anatase and rutile during photocatalysis; the first confines photocatalysis reaction zone within the radius of diffusing $^{\bullet}OH$, and the second on $TiO_{2\text{-}NP}$ surface [44]. This

suggests that a $TiO_{2\text{-NP}}$ anatase-rutile photocatalyst is a more appropriate biological simulant as it simulates both direct and long-range *in vivo* interactions of $^{\bullet}OH$. **4.** Most studies investigate $TiO_{2\text{-NP}}$ photocatalytic properties by focusing on $^{\bullet}OH$ generation [45–48], while our $TiO_{2\text{-NP}}$ system is developed as generator of either $^{\bullet}OH$ or $O_2^{\bullet-}$ alone or both.

A graphic representation of the $TiO_{2\text{-NP}}$ system and its reactions are shown in Fig. 1 and described in detail in *Supplementary Material* ***S3.1***. $TiO_{2\text{-NP}}$ system photo-excitation setup is configured by an appropriate wavelength-emitting, beam focusing and temperature-controlled LED (Fig. 2; see detailed description in *Supplementary Material* ***S2.1.1***).

Upon photo-excitation, the $TiO_{2\text{-NP}}$ system generates $TiO_{2\text{-NP}}(e^-/h^+)$ sites that are independent since the e^-/h^+ pair recombines almost instantly very frequently, and only some percentage of the pairs separate before recombining or being involved in further chemistry [49]. The $TiO_{2\text{-NP}}$ system is based on the 1:1 M production of $^{\bullet}OH$ and $O_2^{\bullet-}$ by the well-established excitation mechanism of $TiO_{2\text{-NP}}$ [50,51], where the primary event, leading to $^{\bullet}OH$ and $O_2^{\bullet-}$ formation (Eqs. (8) to (10)), is catalyzed by the excitation energy (hv) of photons (e.g., in the non-ionizing range 370 to 410 nm [52]) that cause the formation of an electron hole (e^-/h^+) pair:

$$TiO_{2-NP} + h\nu \rightarrow e^-(TiO_{2-NP}) + h^+(TiO_{2-NP}) \quad (8)$$

$$e^-(TiO_{2-NP}) + O_2 \rightarrow O_2^{\cdot-} \quad (9)$$

$$h^+(TiO_{2-NP}) + H_2O \rightarrow {}^{\cdot}OH + H^+ + h^0(TiO_{2-NP}) \quad (10)$$

Given $TiO_{2\text{-NP}}$ system's simultaneous production of $^{\bullet}OH$ and $O_2^{\bullet-}$, we present it also in versions for the separate production of either $O_2^{\bullet-}$ (by the scavenging of $^{\bullet}OH$ by its specific scavenger dimethyl sulfoxide-DMSO [53,54]), or $^{\bullet}OH$ (by setting the $TiO_{2\text{-NP}}$ system to be anaerobic, i.e., by displacing dissolved O_2 via Ar-degassing, with, e.g., H^+ acting as an e^- acceptor; $2H^+ + 2e^- \rightarrow H_2$ [55]). However, if the selected biological system must be aerobic, $O_2^{\bullet-}$ can be scavenged by 100 μM oxidized cytochrome *c* or 45 U/ml SOD [56]; the latter case takes place in the presence of H_2O_2 (product of $O_2^{\bullet-}$ dismutation by SOD [57]).

The $TiO_{2\text{-NP}}$ system is calibrated for $^{\bullet}OH$ and $O_2^{\bullet-}$ production rates by indirect methodologies more sensitive than classic EPR [58], which are based on the quantification of the fluorescent 2-OH-terephthalate (HTPA) and 2-OH-ethidium (HEt), produced via the corresponding reactions of $^{\bullet}OH$ and $O_2^{\bullet-}$ with their specific probes terephthalic acid (TPA) [59] and hydroethidine (HE) [60,61]:

$$^{\cdot}OH + TPA \rightarrow HTPA \quad (11)$$

$$2O_2^{\cdot-} + HE \rightarrow HEt \quad (12)$$

Previous studies have measured $^{\bullet}OH$ produced by UV-irradiated TiO_2 using TPA [45,47,48], and non-specifically with 4-hydroxybenzoic acid [46].

$TiO_{2\text{-NP}}$ system's $^{\bullet}OH/O_2^{\bullet-}$ production is studied on various TPA/HE concentrations. Moreover, $^{\bullet}OH$ production kinetics is studied versus that of the Fenton system. $TiO_{2\text{-NP}}$ system's $O_2^{\bullet-}$ production versus that of the XO system was not tested since the XO system has already been studied, using HE, elsewhere [62].

The $TiO_{2\text{-NP}}$ system has been applied on the indicative biological

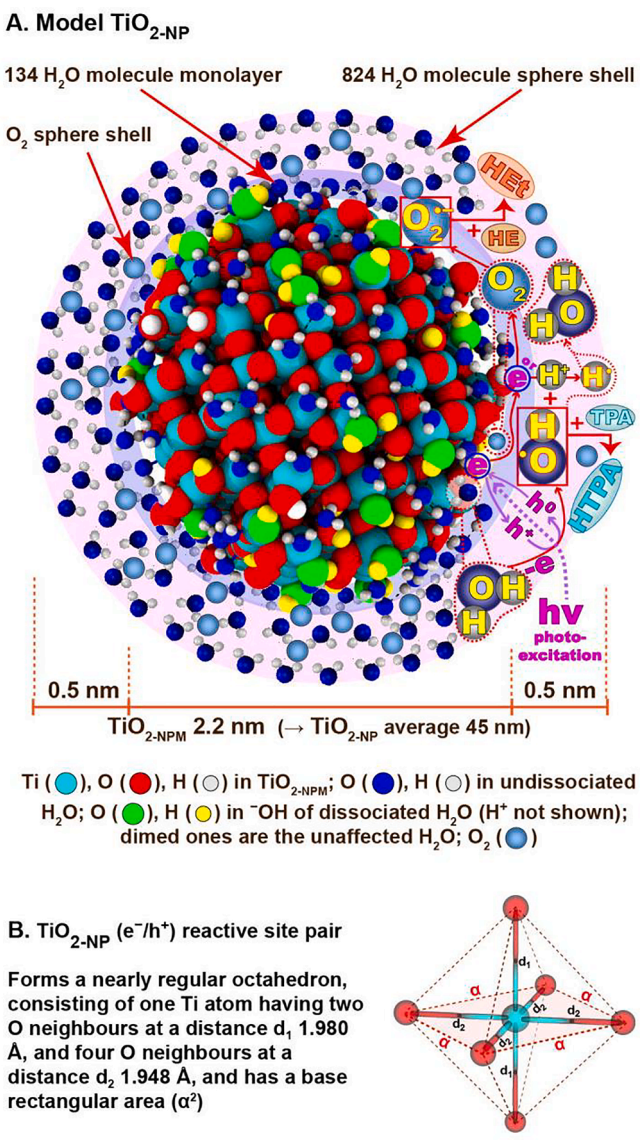

Fig. 1. Photo-excited $TiO_{2\text{-NP}}$ system model and its principles of ROS generation **A.** On the monolayer surface of $TiO_{2\text{-NP}}$ are shown the generated free radicals $O_2^{\bullet-}$ and $^{\bullet}OH$, and their reactions with their corresponding probes HE and TPA (producing HEt and HTPA, respectively), used to calibrate their production rates. **B.** $O_2^{\bullet-}$ and $^{\bullet}OH$ are generated by photo-excited (e^-/h^+) reactive sites located on the surface of $TiO_{2\text{-NP}}$, shown to have an octahedral geometry (see *Supplementary Material* ***S3.1***).

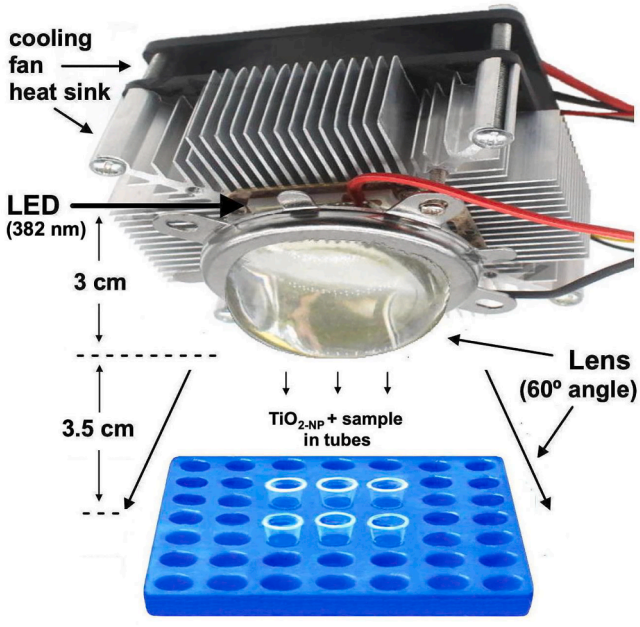

Fig. 2. Photo-excitation setup of the $TiO_{2\text{-NP}}$ system (see detailed description in *Supplementary Material* ***S2.1.1***).

systems BSA and human serum low-density lipoprotein (LDL), by monitoring certain oxidative modifications on them; the former biological system in comparison with the standard Fenton system, and the latter biological system for OS simulation in blood, leading to the formation of oxidized LDL (ox-LDL). BSA is selected as being a model hydrophilic protein, representative of this class in all biological systems. LDL is selected because its structure/components – liposome like, surrounded by a phospholipid layer containing free cholesterol and embedded with the hydrophobic protein apolipoprotein B100 (apoB100), and encapsulating cholesterol esters and triglycerides – are shared by most of the biological systems (cells, membranes, organelles, lipoproteins, proteins, lipids). Moreover, LDL is selected for its medical significance: it is (a) a proven causative factor of atherosclerotic cardiovascular disease (by a mechanism that involves ox-LDL uptake by macrophages [63–65]), (b) linked to atherosclerosis with innate and adaptive immune responses, involving monocytes/macrophages [66] and various T lymphocyte subsets [67], and (c) acting as an autoantigen that can trigger atherosclerosis, thus suggesting an autoimmune basis in the development of the disease [68].

2. Experimental

2.1. Materials

These include reagents, instruments, and standard solutions, the full list of which is presented in *Supplementary Material* ***S1***. Key reagents used are aluminum sulfate hexadecahydrate ($Al_2(SO_4)_3{\cdot}16H_2O$; cat. no. 6421) and dihydroethidium (5-ethyl-5,6-dihydro-6-phenyl-3,8-diaminophenanthridine or hydroethidine or HE; cat. no. 37291) purchased from Fluka. Terephthalic acid (TPA; cat. no. A12527) is purchased from Alfa Aesar. 2-Hydroxy terephthalate (HTPA; cat. no. H1385) is purchased from Tokyo Chemical Industry (TCI). 2-Hydroxy ethidium (2-OH-E^+ or HEt) is synthesized as described elsewhere [61]. Iron (II) sulfate heptahydrate ($FeSO_4{\cdot}7H_2O$, Fe-II; cat. no. F7002) and titanium (IV) oxide nanoparticle ($TiO_{2\text{-NP}}$) dispersion (product cat. no. 700347) are purchased from Sigma-Aldrich (now Merck). $TiO_{2\text{-NP}}$ is a water dispersion of a mixture rutile:anatase 20:80 w/w [69], and 1.3 g/ml density, 33–37 % w/w (455 g/L). The nanoparticle size distribution and characterization of $TiO_{2\text{-NP}}$ is described in *Supplementary Material* ***S3.2***, with nanoparticle size ~ 44 nm being in maximum concentration. All chemicals are of analytical grade, and their standard solutions are prepared from 18.2 mΩ ultra-pure water from a Milli-Q water system (Millipore Corp. Bedford, MA, USA).

2.2. $TiO_{2\text{-NP}}$ system implementation protocol

The development of the $TiO_{2\text{-NP}}$ system for its *in vitro* implementation in various biological systems (see *Procedure* below), is based on certain preliminary investigations briefly outlined as follows (and described in detail in *Supplementary Material* ***S2.1*** and ***S3.1***): (i) $TiO_{2\text{-NP}}$ system modeling based on its physical characteristics (***S3.1***). (ii) effective removal of TiO_2 via precipitation with an appropriate coagulant, and test of possible coprecipitation of proteins (using BSA as a model) (***S2.1.3***); (iii) ranges of $^{\bullet}OH$ and $O_2^{\bullet-}$ production rates by $TiO_{2\text{-NP}}$, in relation to (a) non-ionic wavelength (375–411 nm) excitation [52], (b) irradiation time, and (c) TiO_2 concentration (***S2.1.4***).

2.3. Procedure

Step 1. *Composition of the $TiO_{2\text{-NP}}$ photo-excitation setup*: The setup applied in the present study (Fig. 2) consists of the following parts and operation conditions:

- Heat sink aluminium cooler (for mounting the LED chip), on top of which a cooling fan is mounted. This avoids overheating of the photo-excitation setup and the underneath exposed samples.
- Watt PCB LED, 20-chip-composed, emitting at 382 nm, mounted on the heat sink, with the interface sealed by a thin silicone grease film.
- An optical glass lens with 60° emitting angle, which is mounted on top of the LED via a holder to a beam reflector collimator housing fixed bracket. The resulting photo-excitation setup configuration has the external curved surface of the lens protruding by 3 cm from LED's surface, and at a 3.5 cm distance from the sample tube rack (a total of 6.5 cm from the LED chip surface) as to expose the samples to a light intensity of ~ 50,000 lx. The 60°-irradiation angle of the LED setup allows radiation homogenous co-exposure of up to 8 symmetrically oriented $TiO_{2\text{-NP}}$-containing tubes, so as to also be readily removable upon individual irradiation time interval completion. Excitation setup and samples are isolated from room stray light during irradiation with an appropriate cover.

Step 2. *Setting maximum $TiO_{2\text{-NP}}$ dispersion concentration that ensures its constant homogeneity during set experimental time*: It is known that $TiO_{2\text{-NP}}$ agglomerate and settle down very fast while their sonicated dispersions acquire equilibrium that lasts for certain time at a given temperature, pressure and pH [70]. For setting a maximum concentration of $TiO_{2\text{-NP}}$ dispersion, the criterion we introduce is that the rate of $^{\bullet}OH$ production by this concentration (and lower) of the dispersion, having being pre-sonicated, increases linearly during the set duration time of the sought study. $^{\bullet}OH$ rate vs time is selected since it is not affected by the concentration of the $^{\bullet}OH$ source, H_2O (Eq. (10)), as this is always in excess (55.5 M). In contrast, $O_2^{\bullet-}$ production rate linearity vs time is restricted by the limited concentration of its source, O_2 (Eq. (9)), in H_2O (~260 μM) [71]. This criterion should be met by any source of $TiO_{2\text{-NP}}$ sought to be selected (dispersion, nanopowder, crystal type). In the present study we use the commercial $TiO_{2\text{-NP}}$ as being a mixture of rutile/anatase because the existing localization differences in $^{\bullet}OH$ formation between anatase and rutile during photocatalysis [44] simulate both direct and long-range *in vivo* interactions of $^{\bullet}OH$.

In the present study, the concentration range of TiO_2 (0.04 to 0.32 g/L) is investigated as a function of $^{\bullet}OH$ (and $O_2^{\bullet-}$) rate of production vs time via reaction with TPA (and HE) after photo-excitation of $TiO_{2\text{-NP}}$ at a selected LED wavelength. $^{\bullet}OH$ (and $O_2^{\bullet-}$) rates are determined following the procedures for their quantification described in *Supplementary Material* ***S2.1.4.1***. The 0.12 g/L TiO_2 is selected in the present study because it corresponds to the upper limit of the linear initial rate (V_o) of $^{\bullet}OH$ and $O_2^{\bullet-}$ production (**Fig. S3**).

Step 3. *$^{\bullet}OH$ and $O_2^{\bullet-}$ production calibration for the $TiO_{2\text{-NP}}$ system*: For this, the $TiO_{2\text{-NP}}$ system in the present study is set at final 0.12 g/L TiO_2, and photo-excited at 382 nm with intensity of 50,000 lx. These parameters are determined in *Supplementary Material* ***S2.1.4–5***). $^{\bullet}OH$ and $O_2^{\bullet-}$ are indirectly identified and quantified via their reactions with the corresponding specific probes TPA and HE by the quantification of the corresponding specific fluorescent products, HTPA and HEt, respectively (see Eqs. (11) and (12)), which are tested at various concentrations production rate optimization and kinetics (*section* ***2.4.1***). The following $TiO_{2\text{-NP}}$ system calibration conditions are set for $^{\bullet}OH$ and $O_2^{\bullet-}$, studied either separately or simultaneously, with the probes being omitted when using the $TiO_{2\text{-NP}}$ system in studies on biological systems.

Step 3.1. *$^{\bullet}OH$ production calibration*: For sole $^{\bullet}OH$ production, the system is applied anaerobically, where dissolved O_2 in the reagent/sample solution is removed via Ar-degassing ($O_2^{\bullet-}$ generation is derived from O_2; see Eq. (9)). This method is applied in the present study for kinetics studies, as it does not generate any side products. Alternative methods for eliminating $O_2^{\bullet-}$ are its conversion to (i) O_2 by 100 μM oxidized cytochrome *c* (especially in applications on aerobic biological systems, e.g., cells), and to (ii) O_2 and H_2O_2 by 45 U/ml SOD [56]; in the latter case H_2O_2 (product of $O_2^{\bullet-}$ dismutation by SOD [57]) can be further decomposed to O_2 and H_2O by 20 U/ml catalase [72].

The $TiO_{2\text{-NP}}$ system in addition to its 0.12 g/L in TiO_2 contains TPA in 5 mM excess (determined in *section* ***2.4.1.1***), and is prepared as follows for six photo-exposure time intervals and six corresponding controls: A

12-ml mixture solution made of 9 ml ddH_2O and 3 ml 20 mM TPA, is degassed by Ar-bubbling (for 5 min), and split into two sets of six 1-ml placed in 2-ml-microcentrifuge tubes (corresponding to irradiation time 0.5, 1, 2, 3, 4, 5 min), one designated for samples and one for time-corresponding controls. Ar-degassed samples do not need re-degassing exposed to atmospheric air less than 30 min. To each of the six sample tubes is added 20 μl 6 g/L TiO_2 standard solution (also Ar-degassed for 5 min) prior irradiation, and to the six control tubes the same TiO_2 standard solution is added after irradiation completion. Such control cancels out any possible light irradiation effect, and also interference by any remnants of $TiO_{2\text{-NP}}$ after its removal by precipitation; see step **4**. Both sets of tubes are irradiated as described in step **1**. For $^{\bullet}OH$ production (measured as HTPA) calibration completion follow step **4** and step **5.1**. For applying this step in biological/biochemical studies see *Guidelines* below:

a. The above calibration step is required to verify/control $^{\bullet}OH$ production when using $TiO_{2\text{-NP}}$ system in any study.
b. TPA is tested at various concentrations for kinetics study shown in *section* ***2.4.1.1***. This testing is also important because it sets minimum–maximum TPA concentration range options, especially when the $TiO_{2\text{-NP}}$ system is applied in $^{\bullet}OH$ scavenging studies.
c. After $^{\bullet}OH$/TPA-calibration, the same step can be applied in the absence of TPA and its replacement with the biological sample when studying on it the oxidative effect of $^{\bullet}OH$.

Step 3.2. *$O_2^{\bullet-}$ production calibration*: For sole $O_2^{\bullet-}$ production, the system is applied in presence of the $^{\bullet}OH$ scavenger DMSO at 50 mM, 13-fold less than its biologically non-destructive concentration limit [73]. The $TiO_{2\text{-NP}}$ system in addition to its 0.12 g/L in TiO_2 contains HE in 0.3 mM excess (determined in *section* ***2.4.1.3***), and is prepared as follows for six photo-exposure time intervals and six corresponding controls: The sample set consists of six 2-ml-microcentrifuge tubes (each for 0.5, 1, 2, 3, 4, 5 min irradiation), to which are added (and mixed), in the stated order, 780 μl ddH_2O, 135 μl ACN, 50 μl 1 M DMSO, 15 μl 20 mM HE, and 20 μl 6 g/L TiO_2 (final 50 mM DMSO to scavenge $^{\bullet}OH$, 15 % ACN; added to enhance HE solubility). Similarly, the control set is prepared as the sample one, with the exception that the TiO_2 reagent is added after irradiation completion. Such control cancels out any possible light irradiation effect, and also interference by any remnants of $TiO_{2\text{-NP}}$ after its removal by precipitation; see **step 4**. An additional irradiation-unexposed control tube without HE is prepared, to be used for the fluorescent quantification of HEt in step **5.2** (and designated HEt-reagent control). Both sets of tubes are irradiated as described in step **1**. Upon completion of irradiation, unreactive HE is removed via a 3x-wash of all tubes with an equal volume (1 ml) $CHCl_3$/hexane 1:1 by vigorous vortexing for 30 s, followed by centrifugation at 13,000 *g*, for 5 min, at 4 °C, and discarding the bottom organic phase (where HE is partitioned). For $O_2^{\bullet-}$ production (measured as HEt) calibration completion follow step **4** and step **5.2**. For applying this step in biological/biochemical studies see *Guidelines* below:

a. The above calibration step is required to verify/control $O_2^{\bullet-}$ production when using $TiO_{2\text{-NP}}$ system in any study.
b. HE is tested at various concentrations in the kinetics study shown in *section* ***2.4.1.3***. This testing is also important because it sets minimum–maximum HE concentration range options, especially when the $TiO_{2\text{-NP}}$ system is applied in $O_2^{\bullet-}$ scavenging studies.
c. After $O_2^{\bullet-}$/HE-calibration, the same step can be applied in the absence of HE and its replacement with the biological sample when studying on it the oxidative effect of $O_2^{\bullet-}$.

Step 4. *$TiO_{2\text{-NP}}$ removal by flocculation/coagulation*: This step is applied in case $TiO_{2\text{-NP}}$ may interfere in various applications, such as those involving fluorometric or photometric measurements. The 1-ml-containing sample/control tubes from steps **3.1** and **3.2** are treated for 0.12 g/L TiO_2 removal, by addition of 60 μl 1 M Pi-buffer, pH 7.5 (final 50 mM), and 22 μl 0.25 M $Al_2(SO_4)_3$ (final 5 mM, set as described in *Supplementary Material* ***S2.1.3.1***). Then, all tubes are incubated for 15 min at RT, in the dark, by intermittent inversion to speed up coagulation and flocculation of $TiO_{2\text{-NP}}$, which is precipitated by centrifugation at 16,000 *g* for 10 min, at RT. The $TiO_{2\text{-NP}}$-clear supernatants are transferred to new tubes for further treatment. For applying this step in biological/biochemical studies see *Guidelines* below:

a. The $TiO_{2\text{-NP}}$ removal step is applied when $TiO_{2\text{-NP}}$ may interfere in various applications, such as those involving fluorometric or photometric measurements. $TiO_{2\text{-NP}}$ removal is required in the calibration of the $TiO_{2\text{-NP}}$ system for $^{\bullet}OH$ and $O_2^{\bullet-}$ production because it will interfere in the fluorometric quantification of HTPA and HEt generated in steps **3.1** and **3.2**, respectively (see respective steps **5.1** and **5.2**).
b. This step can be also used when studying biomolecules or cell organelles as long as it is tested that they do not co-precipitate with $TiO_{2\text{-NP}}$. Such molecules could be, e.g., artificial/natural organic molecules investigated as $^{\bullet}OH$ or $O_2^{\bullet-}$ scavengers, proteins (such as BSA and insulin, shown in *Supplementary Material* ***S2.1.3.2***) and nucleic acids. Given that coagulated $TiO_{2\text{-NP}}$ can start precipitating at 1,000 *g* for at least 15 min (data not shown), this step can be investigated for application to organelles such as mitochondria (which precipitate above 7,000 *g*) in the presence of increasing ionic strength to minimize $TiO_{2\text{-NP}}$ /organelle interactions.
c. Examples where $TiO_{2\text{-NP}}$ removal step is not necessary are: (i) liposomes, the lipids of which can be extracted in chloroform by the Folch method [74] – in such case $TiO_{2\text{-NP}}$ is separated as in *section* ***2.6.3***; (ii) serum lipoproteins such as human LDL used in the present study, where $TiO_{2\text{-NP}}$ does not affect LDL component (lipids, apoB100) fractionation (see *section* ***2.6.3***). (iii) In a $TiO_{2\text{-NP}}$/cell (isolated from cultures) co-dispersion, cells can be easily separated from $TiO_{2\text{-NP}}$ since they precipitate at ~ 500 *g*, which is much less than the > 10,000 *g* needed for the precipitation of uncoagulated $TiO_{2\text{-NP}}$ (especially when used at less than 0.12 g/L).

Step 5. *Quantification of HTPA and HEt*: The separate procedures are performed as follows:

Step 5.1. *HTPA quantification*: HTPA in ~300 μl of the $TiO_{2\text{-NP}}$-clear supernatants from step **4** (a continuation of step **3.1**) is quantified by measurement of their fluorescence units (FU) values (diluted, if needed, with ddH_2O) at $\lambda_{ex} = 311$, $\lambda_{em} = 425$ nm [59], after subtraction of the FU values of the corresponding time-interval controls. The net FU are converted to HTPA (in μM) using the FU (~330, using Shimadzu, model RF-1501, set at a 10 nm slit width and at low sensitivity) of a 1 μM HTPA standard solution (made by dilution of 5 mM HTPA; shown in *Supplementary Material* ***S1.3***).

Step 5.2. *HEt quantification*: HEt in 300 μl of the $TiO_{2\text{-NP}}$-clear supernatants from step **4** (a continuation of step **3.2**) is quantified by measurement of their FU values (diluted, if needed, with ddH_2O) at $\lambda_{ex} = 480$, $\lambda_{em} = 575$ nm. These are actually the sum (sum-FU) of HEt-FU and ethidium (Et)-FU, an interfering side product [61]. Thus, the FU value of HEt in the 300 μl is indirectly determined via the fluorescence quenching of HEt-FU with the horse radish peroxidase (HRP)/H_2O_2 system [60]. Specifically, in the 300 μl of each supernatant, 25 μl 1 mM H_2O_2 are mixed with 10 μl 0.1 U/μl HRP (by sequential dilutions of the 100 U/μl standard enzyme solution), incubated (by intermittent inversion) for 10 min at RT, and their FU are re-measured at $\lambda_{ex} = 480$, $\lambda_{em} = 575$ nm. HEt-FU are equal to the difference between sum-FU (i.e., before HRP treatment) and Et-FU (i.e., after HRP treatment). Sample net HEt-FU is the difference between sample HEt-FU and corresponding time-interval control HEt-FU. Subsequently, net FU are converted to HEt (in μM) using the FU of 1 μM HEt solution, prepared as follows: A portion (e.g., 1 ml) of the HEt-reagent control (made in step **3.2**) is spiked with 5 μl 0.2 mM HEt standard solution (to set a final of 1 μM), and the FU (~425)

are measured in the spectrofluorometer of use (Shimadzu, model RF-1501, set at a 10 nm slit width and at high sensitivity).

Step 6. *$TiO_{2\text{-}NP}$ system as generator of both $^{\bullet}OH$ and $O_2^{\bullet-}$*: Upon its mandatory calibration step **3**, the $TiO_{2\text{-}NP}$ system can be used in biological studies as generator of both $^{\bullet}OH$ and $O_2^{\bullet-}$. In that case, the $TiO_{2\text{-}NP}$ system is prepared (for, e.g., six sample photo-exposure time intervals and six corresponding controls) as follows: To the sample set of six 2-ml-microcentrifuge tubes (each for, e.g., 0.5, 1, 2, 3, 4, 5 min irradiation), are added to each tube 20 μl 6 g/L TiO_2 and mixed with sample up to 980 μl (H_2O-diluted or not). Similarly, the control set is prepared as the sample one, with the exception that the TiO_2 reagent is added after irradiation completion. Such control cancels out any possible light irradiation effect, and also interference by any remnants of $TiO_{2\text{-}NP}$ if its removal is needed (see step **4**). Both sets of tubes are then irradiated as described in step **1**, and the exposed samples and controls are processed depending to the biological system of study selected.

2.4. *$TiO_{2\text{-}NP}$ system $^{\bullet}OH$ and $O_2^{\bullet-}$ production kinetics, and comparison with the Fenton system*

The above protocol is applied for the investigation whether $^{\bullet}OH$ and $O_2^{\bullet-}$ production kinetics by the $TiO_{2\text{-}NP}$ system, resembles the competition kinetics taking place in biological systems [75]. In that respect, $TiO_{2\text{-}NP}$ system's $^{\bullet}OH$ production kinetics is compared with that of the standard Fenton system, which is modified to be $^{\bullet}OH$-specific (see *section **2.4.2***).

2.4.1. *$TiO_{2\text{-}NP}$ system kinetics*

$TiO_{2\text{-}NP}$ system kinetics is studied for the reaction of $^{\bullet}OH$ and $O_2^{\bullet-}$, separately, at different concentrations of their corresponding probes TPA and HE as follows:

2.4.1.1. $^{\bullet}OH$ production rates as a function of TPA concentration. They are determined at fifteen different TPA concentrations (0.1 mM to 10 mM), irradiation-exposed for 2.5 and 5 min. The experiment uses four sets, each of fifteen 2-ml-microcentrifuge tubes, arranged as follows: 1st and 2nd sample set (correspondingly for 2.5 and 5 min irradiation) consists of fifteen tubes, to which are added (and mixed), in the stated order, ddH_2O (μl)/20 mM TPA (μl) (both solutions prior Ar-deoxygenated for 5 min), 975/5, 968/12.5, 955/25, 943/37.5, 930/50, 918/62.5, 905/75, 880/100, 855/125, 780/200, 730/250, 680/300, 630/350, 580/400, 480/500, followed by the addition to all of 20 μl 6 g/L TiO_2 (also Ar-deoxygenated for 5 min before use). This achieves the final concentrations 0.1, 0.25, 0.5, 0.75, 1, 1.25, 1.5, 2, 2.5, 4, 5, 6, 7.5, 8, 10 mM for TPA. Similarly, 3rd and 4th control sets are prepared as the sample ones, with the exception that the TiO_2 reagent is not present during irradiation and is added upon its completion. All four sets of tubes are irradiated, treated for $TiO_{2\text{-}NP}$ removal onwards, and measured spectrofluorometrically for HTPA quantification as described in *section **2.3***, steps **1**, **4** and **5.1**, respectively.

2.4.1.2. $^{\bullet}OH$ production as a function of time. The 5-min irradiation time does not represent the maximum interval where $^{\bullet}OH$ production is linear as a function of time. Here, we show this linearity function up to 60 min (actually tested up to 120 min; data not shown) at the maximum TPA concentration (5 mM), beyond which $^{\bullet}OH$ production rate reaches a plateau (Fig. 3A, insert), where the produced $^{\bullet}OH$ reacts at excess TPA. For the experiment, a mix (28 ml) of the following solutions is prepared: 21 ml ddH_2O are mixed with 7 ml 20 mM TPA, degassed by Ar-bubbling (for 5 min), and split into two sets of fourteen 2-ml-microcentrifuge tubes (each containing 1 ml mix, corresponding to irradiation time 0.5, 1, 2, 3, 4, 5, 8, 10, 15, 20, 30, 40, 50, 60 min), one designated for samples and one for time-corresponding controls. To the fourteen sample tubes is added 20 μl 6 g/L TiO_2 standard solution (previously Ar-degassed for 5 min) prior irradiation, and to the fourteen control tubes the same TiO_2 standard solution is added after irradiation completion. Both sets of tubes are irradiated, treated for $TiO_{2\text{-}NP}$ removal onwards, and measured spectrofluorometrically for HTPA quantification as described in *section **2.3***, steps **1**, **4** and **5.1**, respectively.

2.4.1.3. $O_2^{\bullet-}$ production rates as a function of HE concentration. They are determined at seven different HE concentrations (0.05 to 0.5 mM), irradiation-exposed for 2.5 and 5 min (due to loss of linearity > 8 min; see preliminary results in *Supplementary Material **S2.1.4.2***). The experiment uses four sets of 2-ml-microcentrifuge tubes arranged as follows: 1st and 2nd sample set, correspondingly for 2.5 and 5-min irradiation, consists of eight tubes (correspondingly for 0.025, 0.05, 0.1, 0.15, 0.25, 0.35, 0.4, 0.5 mM HE), to which are added (and mixed), in the stated order, followed by ddH_2O/100 % ACN/1 M DMSO/20 mM HE (μl/μl/μl/μl): 794/135/50/1.25, 793/135/50/2.5, 790/135/50/5, 788/135/50/7.5, 783/135/50/12.5, 778/135/50/17.5, 775/135/50/20, 770/135/50/25. Last, is added to all 20 μl 6 g/L TiO_2. This achieves the final concentrations 0.025, 0.05, 0.1, 0.15, 0.25, 0.35, 0.4, and 0.5 mM of HE. Similarly, 3rd and 4th control sets are prepared as the sample ones, with the exception that the TiO_2 reagent is added upon irradiation completion. All four sets of tubes are irradiated, treated for unreactive HE and $TiO_{2\text{-}NP}$ removal onwards, and measured spectrofluorometrically for HEt quantification as described in *section **2.3***, steps **1**, **3.2**, **4** and **5.2**, respectively.

2.4.1.4. $O_2^{\bullet-}$ production as a function of time. The 5-min irradiation time does not represent the maximum interval for the linear $O_2^{\bullet-}$ production versus time, but it extends up to 8 min, as we show by the following experiment testing irradiation time up to 20 min. Following the same reasoning as with $^{\bullet}OH$, we select the maximum HE concentration of 0.3 mM, beyond which $O_2^{\bullet-}$ production rate remains constant (Fig. 3B, insert). The experiment uses two sets of 2-ml-microcentrifuge tubes arranged as follows: The sample set consists of ten tubes (each for 0.5, 1, 2, 3, 4, 5, 8, 10, 15, 20 min irradiation), to which are added (and mixed), in the stated order, 780 μl ddH_2O, 135 μl ACN, 50 μl 1 M DMSO, 15 μl 20 mM HE, and 20 μl 6 g/L TiO_2. Similarly, the control set is prepared as the sample one, with the exception that the TiO_2 reagent is added upon irradiation completion. Both sets of tubes are irradiated, treated for unreactive HE and $TiO_{2\text{-}NP}$ removal onwards, and measured spectrofluorometrically for HEt quantification as described in *section **2.3***, steps **1**, **3.2**, **4** and **5.2**, respectively.

2.4.2. *Fenton system kinetics*

For the standard Fenton system to be compared with the $TiO_{2\text{-}NP}$ system in terms of $^{\bullet}OH$ production, we modify it as follows in order to produce only $^{\bullet}OH$:

i. Modification of the standard Fenton system to become specific for $^{\bullet}OH$ production, by the deoxygenation (via Ar-degassing) of all involved reagent solutions in order to eliminate concurrent production of $O_2^{\bullet-}$ (the initiator of Fenton system's other side-reactions; see *section **1***). It is found that $O_2^{\bullet-}$ is generated in the presence of Fe^{2+} (Fe-II; 0.05 to 1 mM) and the absence of H_2O_2 (verified in *Supplementary Material **S2.2.2***). This takes place with a concurrent generation of $^{\bullet}OH$ (only in not degassed solutions), identified as HTPA, the kinetics of which is investigated right below.
ii. Development of an anaerobic Fenton system that uses TPA at final 5 mM (as in *section **2.4.1.2***) to measure $^{\bullet}OH$ production as a rate of HTPA generation versus reaction time.

2.4.2.1. $^{\bullet}OH$ production by anaerobic Fenton as a function of time.. In the Fenton system, we control $^{\bullet}OH$ production by varying Fe-II concentration up to 1 mM Fe-II, and at a constant excess of 2 mM H_2O_2 (also applied in past studies [38,76–79]) and at constant 5 mM TPA

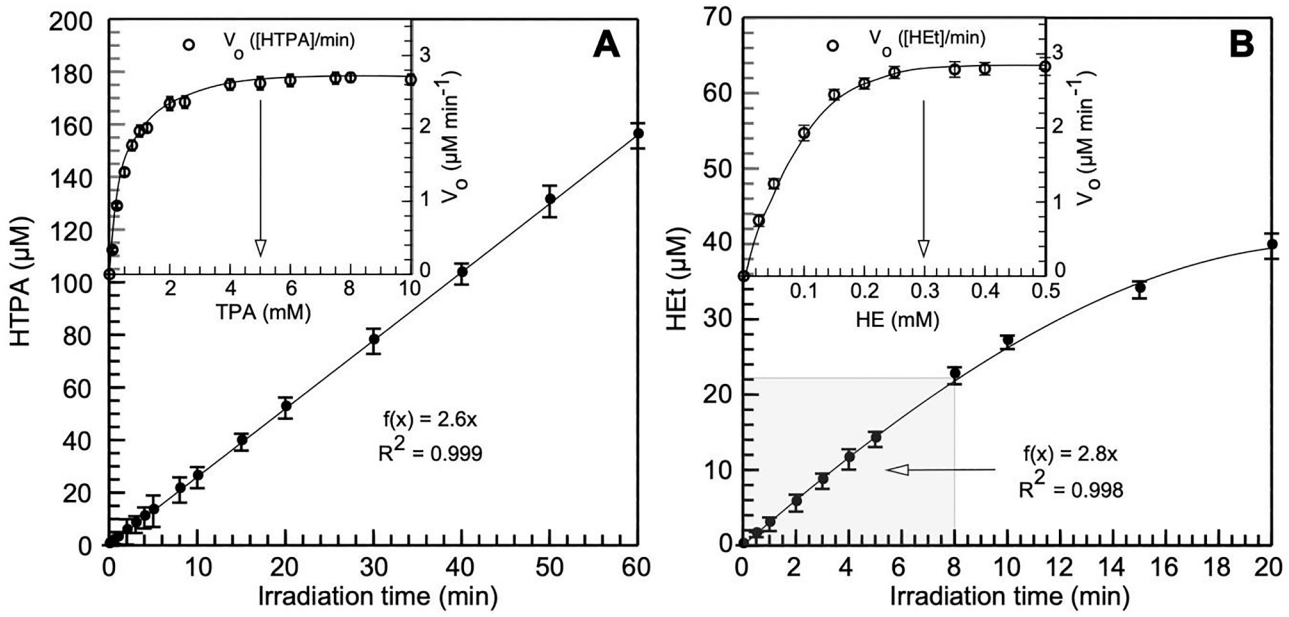

Fig. 3. Kinetics of $^{\bullet}OH$ and $O_2^{\bullet-}$ production by the $TiO_{2\text{-NP}}$ system. **A.** Initial production rate (V_o) of HTPA (thus, of $^{\bullet}OH$) at 5 mM TPA up to 60 min of irradiation; it is actually constant up to at least 2 hrs (data not shown). Insert shows initial production rate velocity (V_o in μM/min; up to 5 min) of HTPA generation by the $TiO_{2\text{-NP}}$ system (using 0.12 g/L TiO_2) versus increasing TPA concentrations; the arrow points to the concentration of TPA (5 mM) at $V_o = V_{max}$. **B.** Initial production rate (V_o) of HEt (thus, of $O_2^{\bullet-}$) at 0.3 mM HE up to 8 min of irradiation, beyond which it starts curving. Insert shows initial production rate velocity (V_o in μM/min; up to 5 min) of HEt by the $TiO_{2\text{-NP}}$ system (using 0.12 g/L TiO_2) versus increasing HE concentrations; the arrow points to the concentration of HE (0.3 mM) at $V_o = V_{max}$. For both A, B, error bars designate SD.

concentration. Specifically, to seven sample 1.5-ml-microcentrifuge tubes the following three solutions are added in the mixing order (in μl/μl/μl), solution TPA-H_2O_2 (7.14 mM TPA + 2.86 mM H_2O_2 + 70 mM Pi-buffer, pH 7.5)/ddH_2O/5 mM Fe-II (the latter added right before fluorescence recordings, as shown below): 350/145/5, 350/135/15, 350/120/30, 350/100/50, 350/90/60, 350/60/90, and 350/50/100

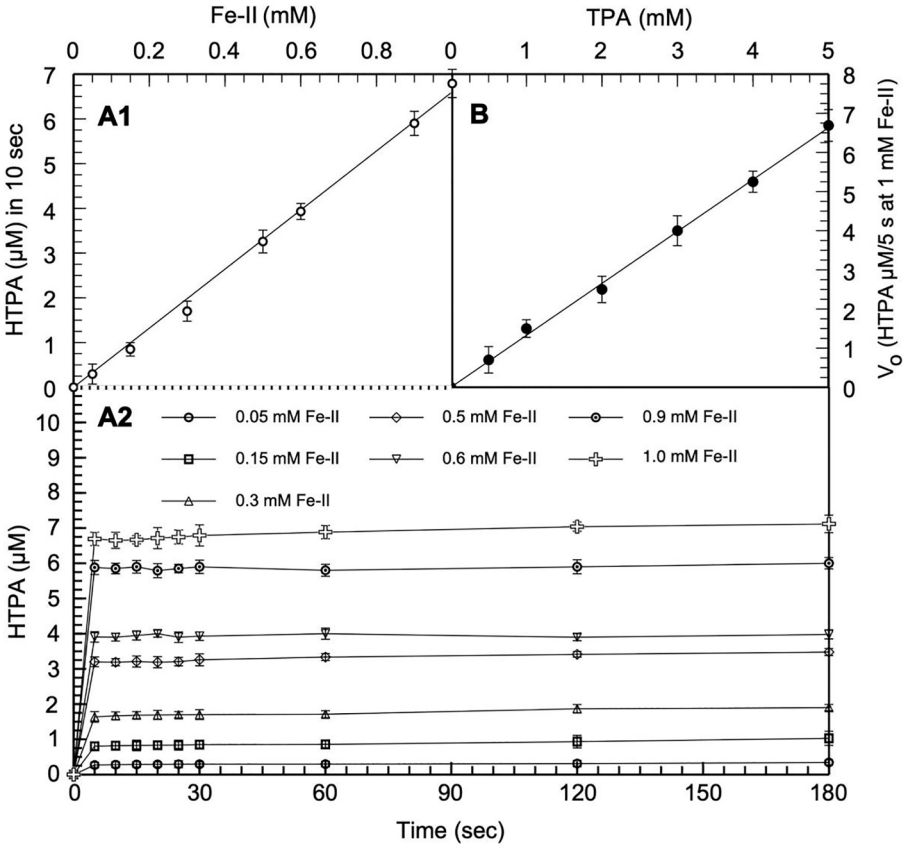

Fig. 4. $^{\bullet}OH$ production by anaerobic Fenton. **A.** Generated $^{\bullet}OH$ is measured as HTPA (formed at 5 mM TPA; same to the TPA concentration which generates V_o $^{\bullet}OH$ production rate plateau in the $TiO_{2\text{-NP}}$ system, see insert in Fig. 3A) at increasing Fe-II concentration: **A1** shows the reaction steady state maximum concentration values of HTPA versus increasing Fe-II concentration, where **A2** shows that these steady state values are reached in 5 s reaction time at all tested Fe-II concentrations. **B.** Production rate initial velocity (V_o) of HTPA (thus, of $^{\bullet}OH$) is attained at the 5 s reaction steady state duration irrespective of the TPA concentrations tested, with Fe-II set at the maximum tested concentration (1 mM). Error bars designate SD.

(all three standard solutions previously Ar-degassed for at least 5 min), to achieve final Fe-II concentrations 0.05, 0.15, 0.3, 0.5, 0.6, 0.9, 1 mM. The corresponding seven control tubes are prepared as the sample ones by replacing solution TPA-H_2O_2 with solution TPA (7.14 mM TPA + 70 mM Pi-buffer, pH 7.5). Each sample and control tube is placed in the cuvette of the spectrofluorometer, followed by the addition of the Fe-II solution and the immediate recording (practically feasible at 5 s after Fe-II addition) of the HTPA FU (at $\lambda_{ex} = 311$, $\lambda_{em} = 425$ nm [59]) up to 3 min. Sample FU's are corrected for the corresponding control FU's, the resulting net FU are converted to μM HTPA (as described in *section* ***2.3***, step **5.1**), which are plotted vs time and vs Fe-II concentration (see Fig. 4A).

2.4.2.2. $^{\bullet}OH$ production rates as a function of TPA concentration.. For the investigation of $^{\bullet}OH$ production kinetics by anaerobic Fenton system with increasing TPA concentration we perform the following experiment. To six sample 1.5-ml-microcentrifuge tubes the following three solutions (together with a 5 mM Fe-II are previously Ar-degassed for at least 5 min) are added in the mixing order (in μl/μl/μl), solution H_2O_2-Pi (4 mM H_2O_2 + 100 mM Pi-buffer, pH 7.5)/20 mM TPA/ddH_2O: 250/12.5/137.5, 250/25/125, 250/50/100, 250/75/75, 250/100/50, and 250/125/25, to achieve final TPA concentrations 0.5, 1, 2, 3, 4, 5 mM, 2 mM H_2O_2 and 50 mM Pi-buffer. The corresponding six control tubes are prepared as the sample ones by replacing solution H_2O_2-Pi with 100 mM Pi-buffer, pH 7.5. Each sample and control tube is placed in the cuvette of the spectrofluorometer, followed by the addition of 100 μl 5 mM Fe-II solution (final 1 mM), and the immediate recording (practically feasible at 5 s after Fe-II addition) of the HTPA FU (at $\lambda_{ex} = 311$, $\lambda_{em} = 425$ nm [59]) up to 3 min. Sample FU's are corrected for the corresponding control FU's, the resulting net FU are converted to μM HTPA (as described in *section* ***2.3***, step **5.1**), which are plotted vs TPA concentration (see Fig. 4B).

2.5. Comparative application of the $TiO_{2\text{-}NP}$ system and the Fenton system on BSA

Given the practically uncontrollable kinetics of the standard Fenton system, even after its modification to produce only $^{\bullet}OH$ (actually, generates both $^{\bullet}OH$ and $O_2^{\bullet-}$, as verified in *Supplementary Material* ***S2.2***; **Fig. S4**), in the present experiment we test comparatively both $TiO_{2\text{-}NP}$ and Fenton systems on BSA, a model protein, under conditions producing both $^{\bullet}OH$ and $O_2^{\bullet-}$. We use BSA to investigate whether this protein undergoes high and/or moderate oxidative modifications by the Fenton system in comparison to the fully controlled $TiO_{2\text{-}NP}$ system. As high oxidative BSA modification is selected its possible fragmentation, evaluated by SDS-PAGE. As indicative moderate oxidative modifications are selected for testing the following oxidative stress markers: di-tyrosines (Tyr-Tyr), protein hydroperoxides (-C—O—O—H), and protein carbonyls (-C═O) formation.

2.5.1. BSA exposure to both $^{\bullet}OH$ and $O_2^{\bullet-}$ by the $TiO_{2\text{-}NP}$ system

Two sets each of nine 2-ml-microcentrifuge tubes are prepared (one for samples and one for controls), corresponding to the irradiation times 5, 10, 15, 20, 30, 40, 60, 90, 120 min. In the sample set, are added, in the stated order, 780 μl ddH_2O, 200 μl 10 mg/ml BSA, and 20 μl 6 g/L TiO_2 (resulting in final 2 mg/ml BSA, and 0.12 g/L TiO_2). The control set is prepared as the sample set with the exception that the 20 μl 6 g/L TiO_2 portions are added upon irradiation completion, meaning $TiO_{2\text{-}NP}$ is not irradiated. An additional control, with BSA and $TiO_{2\text{-}NP}$ not irradiated, is also prepared: It is composed of the same reagents as a sample tube, in order to test the $TiO_{2\text{-}NP}$ removal procedure as possible contributor to the investigated fragmentation and specific oxidative modifications on BSA (see *sections* ***2.5.3*** and ***2.5.4***). The tubes of the two sets are irradiated by the 382 nm LED setup, as described in *section* ***2.3***, step **1**, while during irradiation, the non-irradiated-control tube is kept in the dark. Upon irradiation completion, sample and control tubes are treated for $TiO_{2\text{-}NP}$ precipitation-removal (see *Note*), as described in *section* ***2.3***, step **4**. The resulting control and sample $TiO_{2\text{-}NP}$-free (~1 ml) supernatants are subjected to BSA isolation (by a modification of a protocol described elsewhere [80]) as follows: To each 1-ml-supernatant, are added (and mixed) 25 μl 2.5 mM deoxycholic acid (DOC) and 163 μl 100 % trichloroacetic acid (TCA; final 63.7 μM and 16.3 %, respectively), incubated in an ice-water bath for 20 min, and centrifuged at 13,000 *g* for 5 min at 4 °C. The resulting solid protein pellets are 3x-washed with 0.5 ml cold acetone (while spreading them with the tip of a glass rod), centrifuged after each wash at 13,000 *g* for 5 min (discarding the acetone supernatant), and (after the last wash) evaporated to dryness to form a powder-like protein precipitate. Then the BSA precipitate is solubilized in ~ 200 μl 50 mM NaOH. Before storage at −20 °C, until further analysis (see *sections* ***2.5.3*** and ***2.5.4***), 5 μl from each BSA solubilizate is 20x diluted with ddH_2O, and its protein content is quantified by a sensitive protein quantification assay described elsewhere [81].

Note: In preliminary experiments we have shown that BSA does not co-precipitate with $TiO_{2\text{-}NP}$ (see *Supplementary Material* ***S2.1.3.2***).

2.5.2. BSA exposure to both $^{\bullet}OH$ and $O_2^{\bullet-}$ by the standard Fenton system

BSA (at final 2 mg/ml) is tested by Fenton system at final Fe-II 0.2, 0.6, and 1 mM. Three sets of three 1.5-ml-microcentrifuge tubes (each set representing one of the stated three different Fe-II concentration, at the incubation times 0.5, 1, and 5-min) are prepared as follows: For the 1st set (at 0.2 mM Fe-II), are added, at the stated order, 305 μl ddH_2O, 100 μl 10 mg/ml BSA, 25 μl 1 M Pi-buffer, 50 μl 20 mM H_2O_2, and 20 μl 5 mM Fe-II. For the 2nd set (at 0.6 mM Fe-II), are added, at the stated order, 265 μl ddH_2O, 100 μl 10 mg/ml BSA, 25 μl 1 M Pi-buffer, 50 μl 20 mM H_2O_2, and 60 μl 5 mM Fe-II. For the 3rd set (at 1 mM Fe-II), are added, at the stated order, 225 μl ddH_2O, 100 μl 10 mg/ml BSA, 25 μl 1 M Pi-buffer, 50 μl 20 mM H_2O_2 and 100 μl 5 mM Fe-II. As controls are used (i) 0.5 ml 2 mg/ml BSA minus Fe-II minus H_2O_2, and (ii) 0.5 ml 2 mg/ml BSA minus Fe-II plus H_2O_2, which are justified by the experiment described in *Supplementary Material* ***S2.2***. The reaction in each tube is stopped by the addition of BSA DOC/TCA precipitation reagents (as in *section* ***2.5.1***). Then, BSA in each tube is solubilized and quantified following the protocol described in *section* ***2.5.1***.

2.5.3. Effect of the $TiO_{2\text{-}NP}$ and Fenton systems on BSA fragmentation using SDS-PAGE

This test evaluates whether the $TiO_{2\text{-}NP}$ or Fenton systems produce $^{\bullet}OH$ and $O_2^{\bullet-}$ at near *in vivo* simulation rate ranges, which do not exert extreme destructive effects, such as fragmentation, on proteins, using BSA as a model. For the evaluation of BSA fragmentation by either, certain samples are indicatively chosen to be analyzed by. BSA solubilizates are selected as follows, to be subjected to SDS-PAGE (modified from elsewhere [82]): from the $TiO_{2\text{-}NP}$ system (*section* ***2.5.1***), the non-irradiated-control, and the samples at irradiation times 10, 30, 60 and 120 min; from the Fenton system (*section* ***2.5.2***), samples at 0.2, 0.6, 1 mM Fe-II, all incubated for maximum 5 min. Solubilizates are diluted with the sample buffer (to final ~ 3 μg BSA), and loaded to a 4 % stacking gel, stacked over a 10 % separation gel (see preparation of the involved standard solutions in *Supplementary Material* ***S1.3***). Protein bands are visualized by Coomassie brilliant blue staining. Results are shown in Fig. 6A.

2.5.4. Tyr-Tyr, -C—O—O—H and -C═O measurement on BSA exposed to the $TiO_{2\text{-}NP}$ and Fenton systems

BSA sample and control solubilizates from *sections* ***2.5.1*** and ***2.5.2***, are subjected to the following specific oxidation modifications (expressed per mg BSA):

- *Tyr-Tyr:* Appropriate dilutions of samples/controls (100 to 150-fold, using 50 mM Pi-buffer, pH 7.5) are measured by a previously described protocol using a standard curve with synthesized Tyr-Tyr,

both prepared in *Supplementary Material* ***S2.3***. Results of experiments in *sections* ***2.5.1*** and ***2.5.2*** are shown in Fig. 6B.

- *-C—O—O—H:* Appropriate dilutions of samples/controls (7.5 to 15-fold) are measured following a previously described protocol [83]. Results of experiments in *sections* ***2.5.1*** and ***2.5.2*** are shown in Fig. 6C.
- *-C═O:* Appropriate dilutions of samples/controls (5 to 15-fold) are measured following a previously described protocol [80]. Results of experiments in *sections* ***2.5.1*** and ***2.5.2*** are shown in Fig. 6D.

2.6. $TiO_{2\text{-}NP}$ system on LDL oxidation

In the present experiment we test the $TiO_{2\text{-}NP}$ system (its generated $^{\bullet}OH$ and $O_2^{\bullet-}$) on human serum LDL oxidative modifications, such as lipid hydroperoxides (LOOH), free malondialdehyde (FrMDA) on LDL total lipids, and protein bound MDA (PrMDA) and di-tyrosines (Tyr-Tyr) on apolipoprotein B100 (apoB100).

2.6.1. Serum collection and LDL isolation

Human blood sampling is conducted in accordance with the Declaration of Helsinki and is approved by the Ethics Committee of the University Hospital of the University of Patras (no 259/April 06, 2021). All participants provided informed written consent for use of their biologic material in the present study.Blood is collected in 10 ml serum separator tubes (SST) from three healthy male volunteers (middle-aged, subjected to overnight fast), and incubated at RT for 30 min to clot. Then, the SSTs are centrifuged at 3,000 *g* for 10 min, and the resulting ~ 2 ml clear serum is transferred to 2-ml-microcentrifuge tubes. Serum from the three volunteers, 2 ml each, is then used for LDL isolation by heparin precipitation and the resulting soft pellets are dispersed in 0.3 ml phosphate-buffered saline (PBS), pH 7.4, containing 0.7 M NaCl (as previously described [84]); alternatively, they are stored at −80 °C until use in *section* ***2.6.2***.

2.6.2. LDL exposure to the $TiO_{2\text{-}NP}$ system

Each of the 0.3 ml triplicate LDL dispersions is used to prepare the following two sets (one for irradiated samples in the presence of $TiO_{2\text{-}NP}$ and one for irradiated controls in the absence of $TiO_{2\text{-}NP}$): each set consists of six 2-ml-microcentrifuge tubes, corresponding to the irradiation times 0, 5, 10, 15, 30, 60 min. In the sample set, are added, in the stated order, 942 μl ddH_2O, 18 μl 0.7 M NaCl, 20 μl LDL dispersion, and 20 μl 6 g/L TiO_2 (resulting in final 25.7 mM NaCl and 0.12 g/L TiO_2). The control set is prepared as the sample set with the exception that the 20 μl 6 g/L TiO_2 portions are added upon irradiation completion. The tubes of the two sets are irradiated by the 382 nm LED setup as described in *section* ***2.3***, step **1**. After irradiation completion, sample and control tubes are fractionated for lipid and protein isolation as described in the following step.

2.6.3. LDL fractionation after exposure to the $TiO_{2\text{-}NP}$ system

In each control and sample tube immediately upon irradiation are added 148 μl 5.1 M NaCl and 29.5 μl 1 M Pi-buffer, pH 7.5 (resulting in 0.7 M NaCl and 25 mM Pi), and total lipids are extracted by a modification of the standard chloroform/methanol ($CHCl_3$/MetOH) method [74]. Specifically, in each tube are mixed 800 μl $CHCl_3$/MetOH (3:1 v:v) and 2 μl 400 mM butylated hydroxyanisole (BHA)/400 mM butylated hydroxytoluene (BHT), followed by vigorous vortexing and centrifugation at 13,000 *g* for 5 min at 4 °C, resulting in a bottom (lipid) $CHCl_3$ phase, a middle (apoB100 protein) disk, and a top aqueous-MetOH phase (the latter two containing TiO_2). The bottom phase is collected in a 2-ml-microcentrifuge tube, and to the aqueous/protein phases are added 533 μl $CHCl_3$ and 1 μl 400 mM BHA/400 mM BHT, followed by vigorous vortexing and centrifugation at 13,000 *g* for 5 min at 4 °C. The bottom lipid phase is collected and combined with the first, and evaporated resulting in the total LDL lipids, which are stored at −20 °C until further analysis as in *section* ***2.6.4***. The aqueous phase is also collected in a 2-ml-microcentrifuge tube and immediately treated as in *section* ***2.6.4***. The apoB100 disk is 3x-washed with 0.5 ml cold acetone (while dispersing it with the help of the tip of a glass rod and of a sharp metal spatula) and centrifuged after each wash at 13,000 *g* for 5 min, at 4 °C (discarding the acetone supernatant). The apoB100 pellet after the last wash is evaporated to dryness as to form a powder-like protein precipitate, which is solubilized in ~200 μl 200 mM DOC-Pi pH 7.5 for 3 h (by rotational mixing at RT in the dark) by a modification of a previous study [85], followed by centrifugation at 13,000 *g* for 5 min at 4 °C to precipitate any insoluble $TiO_{2\text{-}NP}$ traces. Before −20 °C storage until further analysis as in *section* ***2.6.4***, 5 μl from each apoB100 solubilizate is 20x diluted with ddH_2O, and its protein content is quantified as described elsewhere [81].

2.6.4. LOOH, FrMDA, PrMDA, and Tyr-Tyr measurement on LDL fractions exposed to the $TiO_{2\text{-}NP}$ system

The isolated LDL fractions are tested for the following oxidative modifications, and expressed per mg apoB100:

- *LOOH*: The total lipids from *section* ***2.6.3*** are solubilized with 20 μl butanol (ButOH) to which are added 80 μl MetOH and kept in an ice-water bath. Appropriate dilutions of samples/controls (20 to 200-fold, using MetOH) are measured by a previously described protocol [83]. Results are shown in Fig. 6E.
- *FrMDA*: Appropriate dilutions of sample/control aqueous phases (1 to 5-fold) from *section* ***2.6.3*** are measured following a previously described protocol [83]; any $TiO_{2\text{-}NP}$ traces do not interfere since the assay detection end-product is extracted/measured in ButOH. Results are shown in Fig. 6F.
- *PrMDA*: Appropriate dilutions of sample/control apoB100 solubilizates (5 to 15-fold, in 0.1 M NaOH, at constant 40 mM DOC) from *section* ***2.6.3*** are measured following a previously described protocol [83]. Results are shown in Fig. 6G.
- *Tyr-Tyr*: Appropriate dilutions (30 to 60-fold, at constant 6 mM DOC) of sample/control apoB100 solubilizates from *section* ***2.6.3*** are measured by a standard curve with synthesized Tyr-Tyr (see *Supplementary Material* ***S2.3***). Results are shown in Fig. 6H.

2.7. Statistical analysis

All data presented are from three independent experiments, and those in Figs. 3, 4, 6 are mean ± standard deviation (SD) using the statistical package SPSS Inc, 2001, release 11.0.

3. Results and discussion

TiO_2 nanoparticles have been used to produce ROS in several applications spanning different scientific fields, using UV-ionizing radiation/solar light for excitation. Indicatively, $TiO_{2\text{-}NP}$ have been used mainly as $^{\bullet}OH$ generator in wastewater oxidative treatment [86–88], in medicine [43] and in biological applications such as *E. coli* inactivation [89] and prion degradation [90]. However, TiO_2 use as $^{\bullet}OH$ source in biological simulations has been limited in studies on antioxidant capacity of certain biomolecules [45,46], where $O_2^{\bullet-}$ was not accounted for, nor the removal of TiO_2.

In the present study we develop a $TiO_{2\text{-}NP}$ system calibrated for the production of $^{\bullet}OH$ and $O_2^{\bullet-}$ alone or both (see *Procedure*'s step **3** in *section* ***2.3***), previously set at 0.12 g/L TiO_2 maximum optimum concentration (see *Procedure*'s step **2** in *section* ***2.3***), and we compare it with the Fenton system in terms of, (a) $^{\bullet}OH$ kinetic rates (Figs. 3 and 4) (and other side reactions, including $O_2^{\bullet-}$ co-generation, see *Supplementary Material* ***S2.2*** and **Fig. S4**), and (b) their comparative oxidative effect on BSA (Fig. 6A-D). Moreover, the $TiO_{2\text{-}NP}$ system is also tested as oxidation simulant on the important biological system of human serum LDL (Fig. 6E-H).

3.1. Kinetics of $^{\bullet}OH$ and $O_2^{\bullet-}$ production by the $TiO_{2\text{-NP}}$ system, and comparison of its $^{\bullet}OH$ kinetics with that of Fenton system

$^{\bullet}OH$ and $O_2^{\bullet-}$ production kinetics by the $TiO_{2\text{-NP}}$ system is investigated whether it resembles the competition kinetics taking place in biological systems [75], and is compared ($^{\bullet}OH$ production) with that of the standard Fenton system, the only one available for simulation studies involving $^{\bullet}OH$ oxidative effects, which is modified to be $^{\bullet}OH$-specific (see *section* ***2.4.2***).

The kinetics of $^{\bullet}OH$ and $O_2^{\bullet-}$ production by the photo-excited $TiO_{2\text{-NP}}$ system is performed via their respective reactions with the specific probes TPA and HE and measured by the respective fluorescent products HTPA and HEt (Fig. 3). The kinetics expressed as μM HTPA/HEt vs irradiation time (min) are linear at 5/0.3 mM TPA/HE, and at least up to 60 min for HTPA (Fig. 3A) and up to 8 min for HEt (Fig. 3B). This linearity is tested at a TPA/HE concentration range 0–10/0–0.5 mM. For the restricted constant generation rate of HEt, the most likely causative factor may be the gradual decrease of dissolved O_2 (irrespective of prior saturation of solutions with O_2, attained by O_2-bubbling until reaching oxygen meter plateau; data not shown). The reason being, O_2 is reduced in time to $O_2^{\bullet-}$ by e^- that are generated by $TiO_{2\text{-NP}}(e^-/h^+)$ (see Eq. (9) in *section* ***1***). It is concluded that the controlled linear increase of $^{\bullet}OH$ and $O_2^{\bullet-}$ production by the photo-excited $TiO_{2\text{-NP}}$ system over extended time (at least 60 min and up to 8 min, respectively) allows the study $^{\bullet}OH/O_2^{\bullet-}$ dose–response-depended oxidative modifications in biological systems.

The kinetics of $^{\bullet}OH/O_2^{\bullet-}$ initial velocity (V_o) production versus TPA/HE concentration is shown in the inserts in Fig. 3, and follows a rectangular hyperbola curve for both probes, which is typical of competition kinetics. The possible photo-excited $TiO_{2\text{-NP}}$ competition kinetics model describing such curve is investigated in *Supplementary Material* ***S3.3***. The possible competition kinetics between the photo-excited $TiO_{2\text{-NP}}$ and $^{\bullet}OH/O_2^{\bullet-}$ for TPA/HE not only signifies the system as simulant for the intra/extra-cellular sources of $^{\bullet}OH/O_2^{\bullet-}$, but also signifies its calibrating reagents TPA/HE as possible simulants of biological organic molecules in their *in vivo* indiscriminate interaction with $^{\bullet}OH/O_2^{\bullet-}$. These dual simulation actions of the $TiO_{2\text{-NP}}$ system make it best suitable for biological simulations.

In comparing kinetically the $TiO_{2\text{-NP}}$ system with the Fenton system, we took into account that the standard Fenton system is typically employed in the presence of dissolved atmospheric O_2 (~200 μM). This does not account for the fact O_2 can react with Fe-II (tested in the present study up to 1 mM, Fig. 4) and produce $O_2^{\bullet-}$ (see Eq. (2)), the dismutation of which generates H_2O_2. The latter in turn is converted to $^{\bullet}OH$ via the Fenton reaction (see Eq. (1)). Indeed, we verified production of $O_2^{\bullet-}$ as shown in *Supplementary Material* ***S2.2***. Therefore, we studied more accurately the kinetics of the Fenton system under anaerobic conditions (for exclusive $^{\bullet}OH$ production) vs the Ar-degassed $TiO_{2\text{-NP}}$ system (to exclusively produce $^{\bullet}OH$) using for both the TPA probe. We regulate the $^{\bullet}OH$ production rate of the anaerobic Fenton by varying Fe^{2+} (Fe-II) concentration (0.05 to 1 mM) at fixed 2 mM H_2O_2. Given the (near diffusion rate) 2nd order $k_{\bullet OH/TPA}$ 3.3×10^9 $M^{-1}s^{-1}$ for the non-enzymic reaction of TPA with $^{\bullet}OH$ [91], we quantified the latter indirectly by measuring the production rate of HTPA (at 5 mM TPA, as established in Fig. 3) in order to compare it with the same type kinetics we applied for the Ar-degassed $TiO_{2\text{-NP}}$ system (Fig. 3A). The kinetics of $^{\bullet}OH$ production versus time at various Fe-II concentrations by the anaerobic Fenton is shown in Fig. 4A. The production rate of $^{\bullet}OH$ reaches reaction steady state (and thereafter a plateau) in 5 s irrespective of Fe-II concentration tested; in comparison to $^{\bullet}OH$ production vs time by the Ar-degassed $TiO_{2\text{-NP}}$ system which is linear up to at least 60 min (Fig. 3A). Moreover, each plateau represents only ~ 0.7 % of the theoretical maximum concentration, which is equimolar to the Fe-II concentration used. Therefore, the recorded HTPA concentrations can be considered the ones having survived oxidation from the generated $^{\bullet}OH$ production burst. The kinetics of $^{\bullet}OH$ initial velocity (V_o) production versus TPA concentration follows a linear curve (Fig. 4B), which is not indicative of a competition kinetics occurring in cells such as that represented by the photo-excited $TiO_{2\text{-NP}}$ (insert in Fig. 3A).

Thus, even the modified Fenton system produces $^{\bullet}OH$ at a very fast steady state (in ~5 s) regardless of varying Fe-II concentration (Fig. 4A), which does not allow the study of longer range $^{\bullet}OH$ dose-response-depended oxidative modifications in biological systems. This together with the non-competitive kinetics of the Fenton system (Fig. 4B) render it inappropriate for $^{\bullet}OH$ simulation studies on biological systems. Given the Fenton system's $^{\bullet}OH$ production peaking in a very short time period (~5 s), any oxidative effects recorded beyond that time in past studies using the standard Fenton system on biological systems [38,79,92–100] cannot be dose-dependent and due to $^{\bullet}OH$ alone. Instead, these may be caused either by the Fenton's components (H_2O_2, Asc, Fe) combined with associated side reactions (e.g., Eq. (2) to (7)), or/and by the $^{\bullet}OH$-primarily oxidized molecular targets of the biological system of study, acting as secondary OS effectors (e.g., secondary radicals) over time.

The $TiO_{2\text{-NP}}$ system is proposed as a replacement of the Fenton in its potential to also simulate the intracellular/extracellular biochemical interactions of $^{\bullet}OH$ envisioned to take place in cellular surfaces interconnected with the dense cytoskeleton. In support to this, the corresponding probes TPA and HE of $^{\bullet}OH$ and $O_2^{\bullet-}$ used for determining their reaction rates (Fig. 3) exhibit competitive kinetics interactions with the photo-excited $TiO_{2\text{-NP}}$ (see **Fig. S8** in *Supplementary Material* ***S3.3***).

The $TiO_{2\text{-NP}}$ system can be applied on a wide range of biological systems, such nucleic acids (genes cloned in plasmids etc.), liposomes, drugs, natural/artificial organic molecules and liquids/extracts as potential antioxidants, cells (e.g., cancer) and organelles, proteins, body fluids, blood serum and lipoproteins (Fig. 5). In the present study, the $TiO_{2\text{-NP}}$ system is applied on indicative biological systems such as the human lipoprotein LDL and the model protein BSA, with the latter comparatively tested with the standard Fenton system.

3.2. $TiO_{2\text{-NP}}$ system application on BSA (vs Fenton system) and on LDL

The $TiO_{2\text{-NP}}$ system-producer of $^{\bullet}OH/O_2^{\bullet-}$, is tested on BSA for comparison with the standard Fenton system $^{\bullet}OH/O_2^{\bullet-}$ version, as

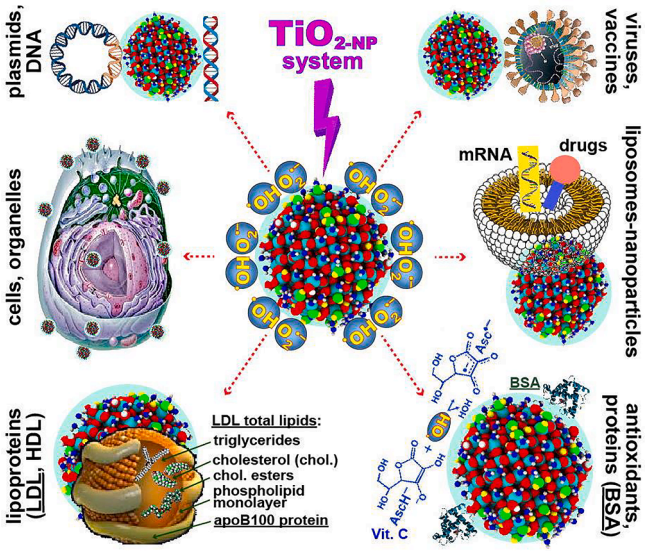

Fig. 5. Indicative *in vitro* high OS biological simulations by the $TiO_{2\text{-NP}}$ system photo (370–410 nm)-excited to generate $^{\bullet}OH$ and $O_2^{\bullet-}$ radicals. Draws depict the average size of the commercial $TiO_{2\text{-NP}}$ (44 nm) in a proportional approximation with the size of the biological systems; indicative sizes: plasmid 20 nm [101], virus 30–1000 nm [102], human cell 10 μm [102], mitochondrion ~ 1 μm diam, 4–10 μm length [103], liposomes 30–350 nm [104], human LDL subclass L3 22 nm, L2 20.5 nm, L1 19 nm [105], proteins 2–11 nm [106]. Underlined biological systems/components were tested in the present study.

shown in *Supplementary Material* ***S2.2***. The kinetics of $^{\bullet}OH$ production by the $TiO_{2\text{-}NP}$ system and the standard Fenton system is tested on the oxidation of BSA, using the following twofold oxidation level analysis: (a) a high oxidative modification one, by evaluating BSA fragmentation using SDS-PAGE; (b) a moderate oxidative modification one, by measuring the oxidative modifications Tyr-Tyr, protein hydroperoxides (-C—O—O—H), and protein carbonyls (-C═O). In terms of high oxidative modifications on BSA, SDS-PAGE in Fig. 6A clearly shows that the $TiO_{2\text{-}NP}$ system does not cause any noticeable fragmentation on BSA, even after 2 h-exposure. In contrast, the standard Fenton system causes substantial fragmentation on BSA with increasing Fe-II concentration (0.2 to 1 mM); fragmentation smearing vs increasing Fe-II concentration reaches near one half the MW of BSA (noticeable from 0.6 mM Fe-II).

In reference to the moderate oxidative modifications on BSA caused by the $TiO_{2\text{-}NP}$ system, there is a time dependent linear increase for Tyr-Tyr/-C—O—O—H/-C═O oxidative modifications at near 40 min exposure (Fig. 6B-D). However, Tyr-Tyr fluorescence-evaluated modification levels follow a gradual decrease thereafter, while the latter two oxidative modifications reach a plateau after 40–60 min. A Tyr-Tyr fluorescence decrease vs irradiation time is also observed when applying the $TiO_{2\text{-}NP}$ system on synthesized Tyr-Tyr alone (see *Supplementary Material* ***S2.4***, **Fig. S5**).

In contrast, for the standard Fenton system, as not being controlled over extended time period (restricted by its very short 5-s kinetic peaking; Fig. 4A2), its produced $^{\bullet}OH$ causes oxidative modification increase on BSA proportional to the increase of Fe-II concentration only for the Tyr-Tyr and -C═O modifications (inserts in Fig. 6B and D). On the other hand, the concentration of -C—O—O—H decreases non-proportionally in reference to incubation time (0.5 to 5 min), while in terms of Fe-II concentration the levels of the same modification peak at 0.6 mM Fe-II followed by a decrease up to the tested 1 mM Fe-II (insert in Fig. 6C). This experimental outcome can be possibly explained by the known reductive reaction of Fe-II with organic hydroperoxides [83,107], which renders the Fenton system inappropriate generator of -C—O—O—H. In reference to the Tyr-Tyr generation on BSA (as well as on the LDL protein apoB100, stated below) with either system, while the role of $^{\bullet}OH$ in the formation of Tyr-Tyr stems from the $^{\bullet}OH$-induced generation of the free radical $Tyr^{\bullet}$ and its subsequent association with a second $Tyr^{\bullet}$ by covalent bond [108], the known role of $O_2^{\bullet-}$ in converting the free radical $Tyr^{\bullet}$ to Tyr [109], may slow down the generation of Tyr-Tyr. Nonetheless, both systems generate 3 (or 33 %) Tyr-Tyr moles per BSA mole (not accounting for possible formation of BSA-BSA Tyr-Tyr-crosslinks), out of the existing total 21 Tyr moles per BSA mole [110].

As already noted in *Introduction*, human serum LDL is chosen as being an important biological sub-system with structural components common in most biological systems, and as involved in many diseases. Therefore, LDL is a biological system appropriate for simulating certain oxidative modifications (LOOH, FrMDA, PrMDA, Tyr-Tyr) on its total lipids and apoB100 caused by $^{\bullet}OH$ and $O_2^{\bullet-}$ simultaneously generated via the $TiO_{2\text{-}NP}$ system. This test also represents a simulation of oxidative stress by $^{\bullet}OH/O_2^{\bullet-}$ sources in blood possibly exerted on circulating LDL.

In reference to LDL lipids, LOOH and FrMDA oxidative modification increasingly linear levels vs irradiation time start curving at 30 min and beyond (Fig. 6E and F). Regarding the LDL protein apoB100, the PrMDA levels show a biphasic linear increase vs irradiation time, with an inflection point near 15 min (Fig. 6G). In contrast, the linear vs irradiation time Tyr-Tyr fluorescence-evaluated modification levels peak at near 20 min, followed by a gradual decrease (Fig. 6H), which is also observed when applying the $TiO_{2\text{-}NP}$ system on synthesized Tyr-Tyr alone (see *Supplementary Material* ***S2.4***, **Fig. S5**). Nonetheless, the $TiO_{2\text{-}NP}$ system generates on apoB100 0.35 (or 2 %) Tyr-Tyr moles per apoB100 mole out of the existing total 33 Tyr moles per apoB100 mole [111].

It should be noted that the $TiO_{2\text{-}NP}$ system causes a linear increase of all the tested oxidative modifications on both BSA and LDL for irradiation exposure 20 to 40 min, which strongly suggests that they are mainly $^{\bullet}OH$ dose-proportional. This is supported by the fact that $^{\bullet}OH$ production rate linearity extends to at least 60 min, while that of $O_2^{\bullet-}$ is up to 8 min. Such an oxidative modification rate profiling caused by the $TiO_{2\text{-}NP}$ system is suggestive of a gradual depletion of existing oxidation-prone modification groups on BSA and LDL, without concomitant fragmentation phenomena (as observed with BSA by the Fenton system).

4. Conclusions

The present study introduces a $TiO_{2\text{-}NP}$ system for the generation of $^{\bullet}OH$ and $O_2^{\bullet-}$ upon visible photo-excitation, in order to be used for high OS biological simulations *in vitro*, the main novelties of which are the following:

- The $TiO_{2\text{-}NP}$ system is set to produce $^{\bullet}OH$ and $O_2^{\bullet-}$ alone or both, instead of its past $^{\bullet}OH$-based (with $O_2^{\bullet-}$ ignored) common use. These options cover all possible generation means of these radicals in biological systems *in vivo*.
- An additional advantage in using $TiO_{2\text{-}NP}$ is its known non-specific electrostatic interactions with H_2O and various biological systems (e.g., cells, membrane proteins, even drugs), which simulate direct/distant interactions of any *in vivo* $^{\bullet}OH$ and $O_2^{\bullet-}$ sources with extra/intracellular biological targets, which take place in a densely packed biomolecular environment. Moreover, the rutile:anatase constitution of the $TiO_{2\text{-}NP}$ system used in the present study simulates both direct and long-range *in vivo* interactions of $^{\bullet}OH$, because of localization differences in its formation between anatase and rutile during photocatalysis [44].
- The $TiO_{2\text{-}NP}$ system can use any commercially available $TiO_{2\text{-}NP}$ source (dispersion, nanopowder, crystal type), as long as $TiO_{2\text{-}NP}$' selected concentrations meet the criterion to produce $^{\bullet}OH$ proportional to irradiation time set for a given simulation study; calibrated by a standardized protocol (*section* ***2.3***) we developed to be applicable to most biological systems (Fig. 5). The protocol offers the option of $TiO_{2\text{-}NP}$ removal via coagulation when needed (e.g., cell organelles, proteins, nucleic acids and other biomolecules).
- The production rates of $^{\bullet}OH$ and $O_2^{\bullet-}$ by the $TiO_{2\text{-}NP}$ system are calibrated with high accuracy, using the respective specific probes TPA and HE, and in comparison to the $^{\bullet}OH$-producing Fenton system. Reaction kinetics of the $TiO_{2\text{-}NP}$ system with these radicals is found to be in competition with their generating source, the $TiO_{2\text{-}NP}$ system. Similar ROS source competition phenomena with biological targets (simulated by TPA/HE) are very common in biological systems. In contrast, the Fenton system is shown not to exhibit such competition kinetics.
- The $TiO_{2\text{-}NP}$ system can be used to study $^{\bullet}OH/O_2^{\bullet-}$ dose–response-depended oxidative modifications in biological simulations. This stems from the fact that $^{\bullet}OH$ and $O_2^{\bullet-}$ linear production rates (60 min and up to 8 min, respectively) can be controlled by varying (i) TiO_2 concentration, (ii) light-source photon emission energy (decreasing from 370 to 410 nm), and (iii) light intensity (as a function of the inverse of squared distance from the irradiated sample). In contrast, $^{\bullet}OH$ production by the Fenton system reaches steady state in ~ 5 s regardless of varying Fe-II concentration, rendering it inappropriate for $^{\bullet}OH$ simulation studies on biological systems.
- The biological simulating potential of the $TiO_{2\text{-}NP}$ system, as producer of both $^{\bullet}OH$ and $O_2^{\bullet-}$, is experimentally verified on indicative biological examples selected to structurally represent most biological systems: BSA as being a model hydrophilic protein, representative of this class in all biological systems; LDL because its structure/components – phospholipid/cholesterol capsule embedded with the hydrophobic protein apoB100, encapsulating cholesterol esters and triglycerides – are shared by most of the biological systems (cells, membranes, organelles, lipoproteins, proteins, lipids) (Fig. 5). The $TiO_{2\text{-}NP}$ system causes a linear increase of all the tested oxidative modifications on both BSA and LDL for irradiation exposure 20 to 40 min, which strongly suggests that they are mainly $^{\bullet}OH$ dose-

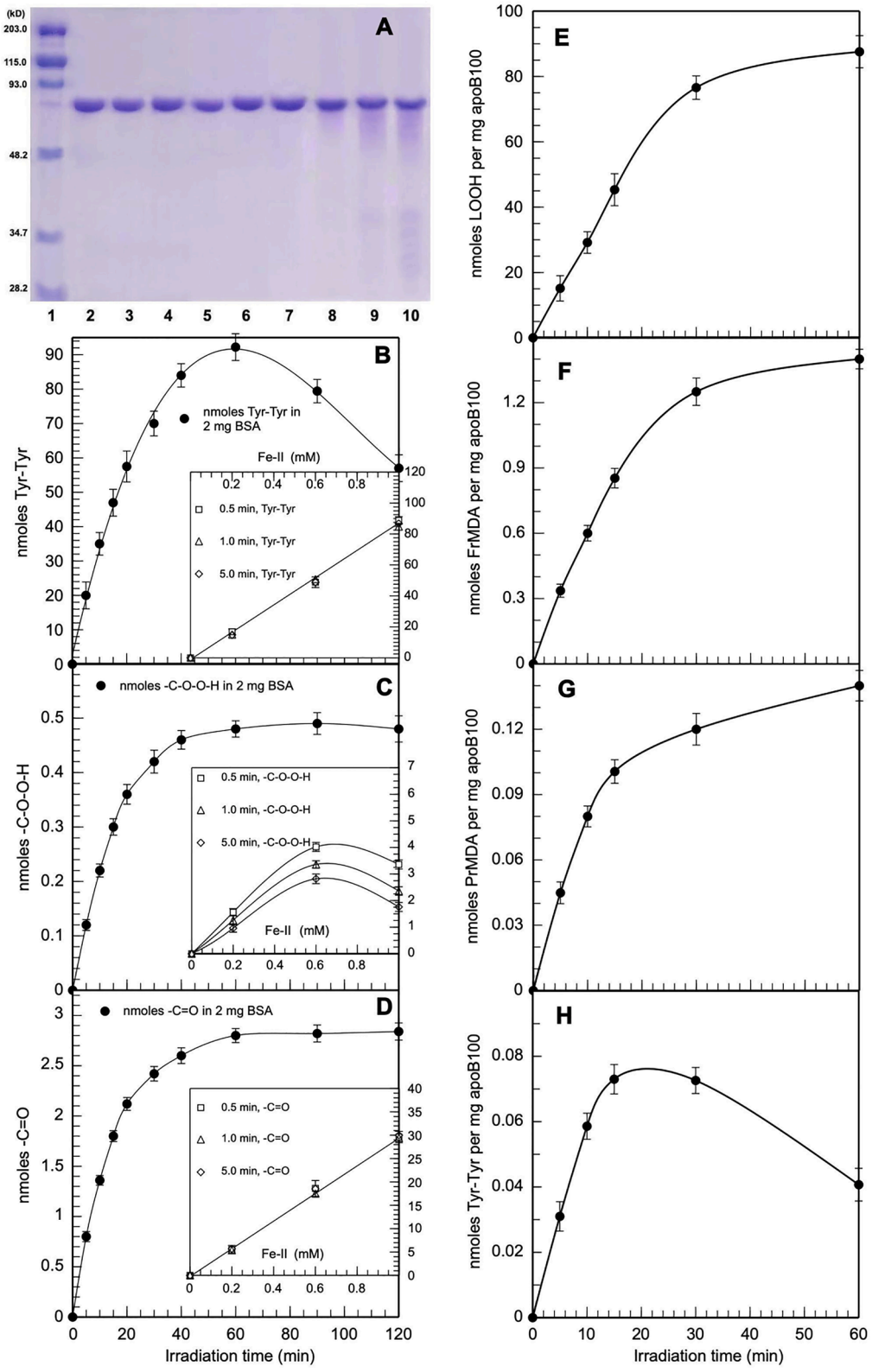

Fig. 6. Evaluation of $TiO_{2\text{-}NP}$ (vs the standard Fenton) system on indicative biological systems: **A.** Comparative SDS-PAGE of BSA exposed to the $TiO_{2\text{-}NP}$ and standard Fenton systems. Band 1 is the molecular weight marker, and control bands 2, and 3, of correspondingly unexposed BSA, and unexposed BSA but exposed to $TiO_{2\text{-}NP}$ treatment. Bands 4, 5, 6 and 7 are for BSA exposed to the $TiO_{2\text{-}NP}$ system for 10, 30, 60, and 120 min, while the bands 8, 9 and 10 are for BSA exposed to the Fenton system at 0.2, 0.6, 1 mM Fe-II (each for 5 min incubation time). Comparative evaluation of the $TiO_{2\text{-}NP}$ and Fenton systems by measuring on BSA the oxidative modifications Tyr-Tyr, -C—O—O—H, and -C═O (**B**, **C**, **D**): **B.** Tyr-Tyr versus exposure time to $TiO_{2\text{-}NP}$ system. Insert shows Tyr-Tyr by Fenton system versus Fe-II concentrations, at three different reaction times (in min). **C.** -C—O—O—H versus exposure time to $TiO_{2\text{-}NP}$ system. Insert shows -C—O—O—H by Fenton system versus Fe-II concentrations, at three different reaction times (in min). **D.** -C═O versus exposure time to $TiO_{2\text{-}NP}$ system. Insert shows -C═O by Fenton system versus Fe-II concentrations, at three different reaction times (in min). Evaluation of the $TiO_{2\text{-}NP}$ system by measuring on LDL the oxidative modifications (**E**, **F**, **G**, **H**): **E.** LOOH; **F.** FrMDA; **G.** PrMDA; **H.** Tyr-Tyr versus irradiation time. Error bars designate SD.

proportional. In contrast, the Fenton system does not display $^{\bullet}OH$ dose-associated oxidative modifications on BSA.

The $TiO_{2\text{-NP}}$ system can serve as replacement of the Fenton system (commonly used for $^{\bullet}OH$ production), in light of its aforementioned limitations. It can also replace other $O_2^{\bullet-}$ producing systems less commonly used, the limitations of which are outlined in the *Introduction* (*section* ***1***). The $TiO_{2\text{-NP}}$ system is currently investigated by our lab in applications measuring total antioxidant capacity (TAC) in any biochemical/biological system (e.g., animal and plant fluids, such as blood serum, eye aqueous humor, plant oils/extracts) selectively against $^{\bullet}OH$ or $O_2^{\bullet-}$. The naturally occurring $^{\bullet}OH$ or $O_2^{\bullet-}$ allow a more accurate measurement of TAC compared to the artificial free radicals used by the currently available TAC methods [112,113].

CRediT authorship contribution statement

Marianna Skipitari: Writing – review & editing, Writing – original draft, Validation, Methodology, Investigation, Formal analysis, Data curation. **Electra Kalaitzopoulou:** Writing – review & editing, Writing – original draft, Methodology, Investigation. **Polyxeni Papadea:** Methodology, Investigation. **Athina Varemmenou:** Methodology, Investigation. **Vassilios E. Gavriil:** Methodology, Investigation. **Evangelia Sarantopoulou:** Methodology, Investigation. **Alkiviadis-Constantinos Cefalas:** Methodology, Investigation. **Sotiris Tsakas:** Methodology, Investigation. **Eleftheria Rosmaraki:** Writing – review & editing, Writing – original draft. **Irene Margiolaki:** Writing – review & editing, Supervision. **Tilman Grune:** Writing – review & editing, Writing – original draft, Resources. **Christos D. Georgiou:** Writing – review & editing, Writing – original draft, Validation, Supervision, Project administration, Methodology, Investigation, Formal analysis, Data curation, Conceptualization.

Declaration of Competing Interest

The authors declare that they have no known competing financial interests or personal relationships that could have appeared to influence the work reported in this paper.

Data availability

All data are available in main article and supplementary material.

Acknowledgements

This work was supported by the Greek Ministry of Education. Part of the research conducted and presented in the present study was supported by the “Andreas Mentzelopoulos Foundation” (PhD Fellowship Grant Number 33720000) of the University of Patras. It was also supported, by the Hellenic Foundation for Research and Innovation (HFRI) under the HFRI PhD Fellowship grant (Fellowship Number 653), and by Greece and the European Union (European Social Fund-ESF) through the Operational Program «Human Resources Development, Education and Lifelong Learning» in the context of the Act “Enhancing Human Resources Research Potential by undertaking a Doctoral Research” Sub-action 2: IKY Scholarship Program for PhD candidates in the Greek Universities.

Appendix A. Supplementary data

Supplementary data to this article can be found online at https://doi.org/10.1016/j.jphotochem.2022.114290.

Reference

[1] A.W. Pryor, The role of free radicals in biological systems, in: A.W. Pryor (Ed.), Free Radicals in Biology, Academic Press, New York, 1976, pp. 1–49.
[2] W.A. Pryor, Oxy-radicals and related species: their formation, lifetimes, and reactions, Annu. Rev. Physiol. 48 (1986) 657–667.
[3] B. Halliwell, J.M.C. Gutteridge, Free Radicals in Biology and Medicine, 5th ed., Oxford University Press, Oxford, 2015.
[4] I. Fridovich, Biological effects of the superoxide radical, Arch. Biochem. Biophys. 247 (1986) 1–11.
[5] T. Kanno, K. Nakamura, H. Ikai, K. Kikuchi, K. Sasaki, Y. Niwano, Literature review of the role of hydroxyl radicals in chemically-induced mutagenicity and carcinogenicity for the risk assessment of a disinfection system utilizing photolysis of hydrogen peroxide, J. Clin. Biochem. Nutr. 51 (1) (2012) 9–14.
[6] X. Wang, L. Zhang, Kinetic study of hydroxyl radical formation in a continuous hydroxyl generation system, RSC Adv. 8 (71) (2018) 40632–40638.
[7] S. Marklund, Spectrophotometric study of spontaneous disproportionation of superoxide anion radical and sensitive direct assay for superoxide dismutase, J. Biol. Chem. 251 (1976) 7504–7507.
[8] B. Chance, H. Sies, A. Boveris, Hydroperoxide metabolism in mammalian organs, Physiolog. Rev. 59 (1979) 527–605.
[9] P.R. Gardner, P.R. Gardner, Superoxide-driven aconitase FE-S center cycling, Biosci. Rep. 17 (1) (1997) 33–42.
[10] S.I. Liochev, I. Fridovich, Superoxide and iron: partners in crime, IUBMB Life 48 (2) (1999) 157–161.
[11] I.O. Aruoma, B. Halliwell, Superoxide-dependent and ascorbate-dependent formation of hydroxyl radicals from hydrogen peroxide in the presence of iron, Biochem. J. 241 (1987) 273–278.
[12] C.M.J. Gutteridge, A.D. Rowley, B. Halliwell, Superoxide-dependent formation of hydroxyl radicals in the presence of iron salts, Biochem. J. 199 (1981) 263–265.
[13] H.J.H. Fenton, Oxidation of tartaric acid in presence of iron, J. Chem. Soc. Trans. 65 (1894) 899–911.
[14] C. Schweikert, A. Liszkay, P. Schopfer, Polysaccharide degradation by Fenton reaction–or peroxidase-generated hydroxyl radicals in isolated plant cell walls, Phytochemistry 61 (1) (2002) 31–35.
[15] R. Milo, R. Phillips, Cell Biology by the numbers, Garland Science, NY, 2015.
[16] G.C. Brown, Total cell protein concentration as an evolutionary constraint on the metabolic control distribution in cells, J. Theor. Biol. 153 (2) (1991) 195–203.
[17] K. Luby-Phelps, Cytoarchitecture and physical properties of cytoplasm: volume, viscosity, diffusion, intracellular surface area, Int. Rev. Cytol. 192 (2000) 189–221.
[18] R. Milo, What is the total number of protein molecules per cell volume? A call to rethink some published values, Bioessays 35 (12) (2013) 1050–1055.
[19] L.R. Barbosa, M.G. Ortore, F. Spinozzi, P. Mariani, S. Bernstorff, R. Itri, The importance of protein-protein interactions on the pH-induced conformational changes of bovine serum albumin: a small-angle X-ray scattering study, Biophys. J. 98 (1) (2010) 147–157.
[20] T. Peters, All About Albumins: Biochemistry, Genetics and Medical Applications, Academic Press, San Diego, CA, 1996.
[21] A. Mogilner, Mechanics of Motor Proteins and the Cytoskeleton, Jonathon Howard Sinauer Associates, Sunderland, Mass, 2001.
[22] A.D. Robertson, Intramolecular interactions at protein surfaces and their impact on protein function, Trends Biochem. Sci. 27 (10) (2002) 521–526.
[23] R.A. Corey, P.J. Stansfeld, M.S.P. Sansom, The energetics of protein-lipid interactions as viewed by molecular simulations, Biochem. Soc. Trans. 48 (1) (2020) 25–37.
[24] C. Peri, G. Morra, G. Colombo, Surface energetics and protein-protein interactions: analysis and mechanistic implications, Sci. Rep. 6 (2016) 24035.
[25] J.G. Watterson, A role for water in cell structure, Biochem J. 248 (2) (1987) 615–617.
[26] F. Haber, J. Weiss, The catalytic decomposition of hydrogen peroxide by iron salts, Proc. Roy. Soc. A 147 (861) (1934) 332–351.
[27] W.G. Barb, J.H. Baxendale, P. George, K.R. Hargrave, Reactions of ferrous and ferric ions with hydrogen peroxide. Part I. —The ferrous ion reaction, Trans. Faraday Soc. 47 (1951) 462–500.
[28] W.G. Barb, J.H. Baxendale, P. George, K.R. Hargrave, Reactions of ferrous and ferric ions with hydrogen peroxide. Part II.—The ferric ion reaction, Trans. Faraday Soc. 47 (1951) 591–616.
[29] Y.H. Hsieh, Y.P. Hsieh, Kinetics of Fe(III) reduction by ascorbic acid in aqueous solutions, J. Agric. Food Chem. 48 (5) (2000) 1569–1573.
[30] A.J. Nappi, E. Vass, Hydroxyl radical production by ascorbate and hydrogen peroxide, Neurotox. Res. 2 (2000) 1029–8428.
[31] Y. Mizuta, T. Masumizu, M. Kohno, A. Mori, L. Packer, Kinetic analysis of the Fenton reaction by ESR-spin trapping, Biochem. Mol. Biol. Int. 43 (5) (1997) 1107–1120.
[32] B. Halliwell, C.M.J. Gutteridge, Oxygen toxicity, oxygen radicals, transition metals and disease, Biochem. J. 219 (1984) 1–14.
[33] G.A. Porras, S.J. Olson, G. Palmer, The reaction of reduced xanthine oxidase with oxygen: Kinetics of peroxide and superoxide formation, J. Biol. Chem. 256 (1981) 9096–9103.
[34] M. Nishikimi, N. Appaji, K. Yagi, The occurrence of superoxide anion in the reaction of reduced phenazine methosulfate and molecular oxygen, Biochem. Biophys. Res. Commun. 46 (2) (1972) 849–854.
[35] X. Li, Improved pyrogallol autoxidation method: a reliable and cheap superoxide-scavenging assay suitable for all antioxidants, J. Agric. Food Chem. 60 (25) (2012) 6418–6424.

[36] A.K. Grover, S.E. Samson, Effect of superoxide radical on Ca^{2+} pumps of coronary artery, Am. J. Physiol. 255 (3 pt 1) (1988) C297–C303.
[37] M. Hara, M. Fujinaga, T. Kuboi, Radical scavenging activity and oxidative modification of citrus dehydrin, Plant Physiol. Biochem. 42 (7–8) (2004) 657–662.
[38] F. Chen, G. Huang, Z. Yang, Y. Hou, Antioxidant activity of *Momordica charantia* polysaccharide and its derivatives, Int. J. Biol. Macromol. 138 (2019) 673–680.
[39] T. Nishino, K. Okamoto, B.T. Eger, E.F. Pai, T. Nishino, Mammalian xanthine oxidoreductase – Mechanism of transition from xanthine dehydrogenase to xanthine oxidase, FEBS J. 275 (13) (2008) 3278–3289.
[40] G. Fazio, D. Selli, L. Ferraro, G. Seifert, C. Di Valentin, Curved TiO_2 nanoparticles in water: short (chemical) and long (physical) range interfacial effects, ACS Appl. Mater. Interfaces. 10 (35) (2018) 29943–29953.
[41] B.M. Rothen-Rutishauser, S. Schurch, B. Haenni, N. Kapp, P. Gehr, Interaction of fine particles and 2. nanoparticles with red blood cells visualized with advanced microscopic techniques, Environ. Sci. Technol. 40 (14) (2006) 4353–4359.
[42] N. Lagopati, P.V. Kitsiou, A.I. Kontos, P. Venieratos, E. Kotsopoulou, A.G. Kontos, D.D. Dionysiou, S. Pispas, E.C. Tsilibary, P. Falaras, Photo-induced treatment of breast epithelial cancer cells using nanostructured titanium dioxide solution, J. Photochem. Photobiol. A: Chem. 214 (2010) 215–223.
[43] N. Lagopati, K. Evangelou, P. Falaras, E.C. Tsilibary, P.V.S. Vasileiou, S. Havaki, A. Angelopoulou, E.A. Pavlatou, V.G. Gorgoulis, Nanomedicine: Photo-activated nanostructured titanium dioxide, as a promising anticancer agent, Pharmacol. Ther. 222 (2021), 107795.
[44] Y. Nosaka, A. Nosaka, Understanding hydroxyl radical ($^{\bullet}OH$) generation processes in photocatalysis, ACS Energy Lett 1 (2) (2016) 356–359.
[45] S.A.V. Eremia, D. Chevalier-Lucia, G.L. Radu, J.L. Marty, Optimization of hydroxyl radical formation using TiO_2 as photocatalyst by response surface methodology, Talanta 77 (2) (2008) 858–862.
[46] Y. Wang, C. Calas-Blanchard, M. Cortina-Puig, L. Baohong, J.L. Marty, An electrochemical method for sensitive determination of antioxidant capacity, Electroanalysis 12 (2009) 1395–1400.
[47] K. Ishibashi, A. Fujishima, T. Watanabe, K. Hashimoto, Detection of active oxidative species in TiO_2 photocatalysis using the fluorescence technique, Electrochem. Commun. 2 (2000) 207–210.
[48] X. Chen, X. Peng, L. Jiang, X. Yuan, J. Zhang, H. Yu, Terephthalate acid decorated TiO_2 for visible light driven photocatalysis mediated via ligand-to-metal charge transfer (LMCT), Colloids Surf. A: Physicochem. Eng. Asp. 603 (2020), 125188.
[49] A.P. Zent, A.S. Ichimura, R.C. Quinn, H.K. Harding, The formation and stability of the superoxide radical (O_2^-) on rock-forming minerals: Band gaps, hydroxylation state, and implications for Mars oxidant chemistry, J. Geophys. Res. 113 (2008) E09001.
[50] S. Munnix, M. Schmeits, Electronic structure of ideal TiO_2(110), TiO_2(001), and TiO_2(100) surfaces, Phys. Rev. [Sect.] B 30 (1984) 2207–2217.
[51] R. Konaka, E. Kasahara, W.C. Dunlap, Y. Yamamoto, K.C. Chien, M. Inoue, Irradiation of titanium dioxide generates both singlet oxygen and superoxide anion, Free Rad, Biol. Med. 27 (1999) 294–300.
[52] C.L. Hawkins, M.J. Davies, Detection, identification, and quantification of oxidative protein modifications, J. Biol. Chem. 294 (51) (2019) 19683–19708.
[53] M.S. Klein, G. Cohen, I.A. Cederbaum, The interaction of hydroxyl radicals with dimethylsulfoxide, FEBS Lett. 116 (1980) 220–222.
[54] C.F. Babbs, M.G. Steiner, Detection and quantitation of hydroxyl radical using dimethyl sulfoxide as molecular probe, in: J.N. Abelson, M.I. Simon (Eds.), Methods in Enzymology, Academic Press, New York, 1990, pp. 137–147.
[55] C.D. Jaeger, A.J. Bard, Spin trapping and electron spin resonance detection of radical intermediates in the photodecomposition of water at titanium dioxide particulate systems, J. Phys. Chem. 83 (24) (1979) 3146–3152.
[56] C.D. Georgiou, D. Zisimopoulos, K. Panagiotidis, K. Grintzalis, I. Papapostolou, R. C. Quinn, C.P. McKay, H. Sun, Martian superoxide and peroxide O_2 release (OR) assay: A new technology for terrestrial and planetary applications, Astrobiology 16 (2) (2016) 126–142.
[57] C.M.J. Gutteridge, Superoxide dismutase inhibits the superoxide-driven Fenton reaction at two different levels, FEBS Lett. 185 (1985) 19–23.
[58] C.D. Georgiou, I. Papapostolou, H. Sun, C.P. McKay, Superoxide radical assays and applications in Mars-like Atacama soils, J. Geophys. Res. 112 (2007) G04S13.
[59] L. Linxiang, Y. Abe, Y. Nagasawa, R. Kudo, N. Usui, K. Imai, T. Mashino, M. Mochizuki, N. Miyata, An HPLC assay of hydroxyl radicals by the hydroxylation reaction of terephthalic acid, Biomed. Chromatogr. 18 (2004) 470–474.
[60] C.D. Georgiou, I. Papapostolou, K. Grintzalis, Superoxide radical detection in cells, tissues, organisms (animals, plants, insects, microorganisms) and soils, Nature Prot. 3 (2008) 1679–1692.
[61] D.N. Zisimopoulos, E. Kalaitzopoulou, M. Skipitari, P. Papadea, N. T. Panagopoulos, G. Salahas, C.D. Georgiou, Detection of superoxide radical in all biological systems by Thin Layer Chromatography, Arch. Biochem. Biophys. 716 (2022), 109110.
[62] J. Chen, S.C. Rogers, M. Kavdia, Analysis of kinetics of dihydroethidium fluorescence with superoxide using xanthine oxidase and hypoxanthine assay, Ann. Biomed. Eng. 41 (2) (2013) 327–337.
[63] H. Itabe, M. Ueda, Measurement of plasma oxidized low-density lipoprotein and its clinical implications, J. Atheroscler. Thromb. 14 (2007) 1–11.
[64] J. Oh, A.E. Riek, S. Weng, M. Petty, D. Kim, M. Colonna, M. Cella, C. Bernal-Mizrachi, Endoplasmic reticulum stress controls M2 macrophage differentiation and foam cell formation, J. Biol. Chem. 287 (15) (2012) 11629–11641.
[65] X.H. Yu, Y.C. Fu, D.W. Zhang, K. Yin, C.K. Tang, Foam cells in atherosclerosis, Clin. Chim. Acta 424 (2013) 245–253.
[66] D. Ferrari, A. la Sala, D. Milani, C. Celeghini, F. Casciano, Purinergic signaling in controlling macrophage and T cell functions during atherosclerosis development, Front. Immunol. 11 (2021), 617804.
[67] S. Lee, B. Bartlett, G. Dwivedi, Adaptive immune responses in human atherosclerosis, Int. J. Mol. Sci. 21 (23) (2020) 9322.
[68] I.I. Cinoku, C.P. Mavragani, H.M. Moutsopoulos, Atherosclerosis: Beyond the lipid storage hypothesis. The role of autoimmunity, Eur. J. Clin. Invest. 50 (2) (2020) e13195.
[69] E. Eymard-Vernain, S. Luche, T. Rabilloud, C. Lelong, Impact of nanoparticles on the Bacillus subtilis (3610) competence, Sci. Rep. 8 (1) (2018) 2978.
[70] V.V. Semashko, M.S. Pudovkin, A.C. Cefalas, P.V. Zelenikhin, V.E. Gavriil, A. S. Nizamutdinov, Z. Kollia, A. Ferraro, E. Sarantopoulou, Tiny rare-earth fluoride nanoparticles activate tumour cell growth via electrical polar interactions, Nanoscale Res. Lett. 13 (1) (2018) 370.
[71] B. Reynafarje, L.E. Costa, A.L. Lehninger, O_2 solubility in aqueous media determined by a kinetic method, Anal. Biochem. 145 (2) (1985) 406–418.
[72] C.D. Georgiou, C.P. McKay, R.C. Quinn, E. Kalaitzopoulou, P. Papadea, M. Skipitari, The Oxygen Release Instrument: Space mission reactive oxygen species measurements for habitability characterization, biosignature preservation potential assessment, and evaluation of human health hazards, Life (Basel) 9 (3) (2019) 70, https://doi.org/10.3390/life9030070.
[73] A.A. Gurtovenko, J. Anwar, Modulating the structure and properties of cell membranes: the molecular mechanism of action of dimethyl sulfoxide, J. Phys. Chem. B 111 (2007) 10453–10460.
[74] J. Folch, M. Lees, H.G. Sloane-Stanley, A simple method for the isolation and purification of total lipids from animal tissues, J. Biol. Chem. 226 (1957) 497–509.
[75] S. Schäuble, A.K. Stavrum, P. Puntervoll, S. Schuster, I. Heiland, Effect of substrate competition in kinetic models of metabolic networks, FEBS Lett. 587 (17) (2013) 2818–2824.
[76] Y. Luo, E.S. Henle, R. Chatopadhyaya, J. Rucheng, S. Linn, Detecting DNA damage caused by iron and hydrogen peroxide, Methods Enzymol. 234 (1994) 51–59.
[77] Y. Luo, E.S. Henle, S. Linn, Oxidative damage to DNA constituents by iron-mediated Fenton reactions. The deoxycytidine family, J. Biol. Chem. 271 (35) (1996) 21167–21176.
[78] C. Baron, H.H.F. Refsgaard, L.H. Skibsted, M.L. Andersen, Oxidation of bovine serum albumin initiated by the Fenton reaction – Effect of EDTA, tert-butylhydroperoxide and tetrahydrofuran, Free Radic. Res. 40 (4) (2006) 409–417.
[79] M. Khosravifarsani, A.S. Monfared, M. Pouramir, E. Zabihi, Effects of Fenton reaction on human serum albumin: an in vitro study, Electron Physician 8 (9) (2016) 2970–2976.
[80] C.D. Georgiou, D. Zisimopoulos, V. Argyropoulou, E. Kalaitzopoulou, G. Salachas, T. Grune, Protein and cell wall polysaccharide carbonyl determination by a neutral pH 2,4-dinitrophenylhydrazine-based photometric assay, Redox Biology 17 (2018) 128–142.
[81] C.D. Georgiou, K. Grintzalis, G. Zervoudakis, I. Papapostolou, Mechanism of Coomassie brilliant blue G-250 binding to proteins: a hydrophobic assay for nanogram quantities of proteins, Anal. Bioanal. Chem. 391 (2008) 391–403.
[82] U.K. Laemmli, Cleavage of structural proteins during the assembly of the head of bacteriophage T4, Nature 227 (5259) (1970) 680–685.
[83] K. Grintzalis, D. Zisimopoulos, T. Grune, D. Weber, C.D. Georgiou, Method for the simultaneous determination of free/protein malondialdehyde and lipid/protein hydroperoxides, Free Radic. Biol. Med. 59 (2013) 27–35.
[84] W.H. Sutherland, Oxidation of heparin-isolated LDL by hemin. The effect of serum components, Arterioscler. Thromb. Vasc. Biol. 14 (1994) 1966–1975.
[85] M.T. Walsh, D. Atkinson, Solubilization of low-density lipoprotein with sodium deoxycholate and recombination of apoprotein B with dimyristoylphosphatidylcholine, Biochemistry (1983) 3170–3178.
[86] M.H. Hazaraimi, P.S. Goh, M.N. Subramaniam, M. Pandiyan, N.D. Suzaimi, W. J. Lau, A.F. Ismail, Silver doped titania nanotubes incorporated photocatalytic dual layer antibiofouling hollow fiber membrane for palm oil wastewater treatment, J. Environ. Chem. Eng. 9 (2021), 106192.
[87] M.R. Al-Mamun, S. Kader, M.S. Islam, Solar-TiO_2 immobilized photocatalytic reactors performance assessment in the degradation of methyl orange dye in aqueous solution, Environ. Nanotechnol. Monit. Manag. 16 (2021), 100514.
[88] M. Penas-Garzon, W.H.M. Abdelraheem, C. Belver, J.J. Rodriguez, J. Bedia, D. D. Dionysiou, TiO_2-carbon microspheres as photocatalysts for effective remediation of pharmaceuticals under simulated solar light, Sep. Purif. Technol. 275 (2021), 119169.
[89] M. Cho, H. Chung, W. Choi, J. Yoon, Linear correlation between inactivation of E. coli and OH radical concentration in TiO_2 photocatalytic disinfection, Water Res. 38 (4) (2004) 1069–1077.
[90] I. Paspaltsis, K. Kotta, R. Lagoudaki, N. Grigoriadis, I. Poulios, T. Sklaviadis, Titanium dioxide photocatalytic inactivation of prions, J. Gen. Virol. 87 (Pt 10) (2006) 3125–3130.
[91] M. Saran, K.H. Summer, Assaying for hydroxyl radicals: hydroxylated terephthalate is a superior fluorescence marker than hydroxylated benzoate, Free Radic. Res. 31 (1999) 429–436.
[92] S. Guedes, R. Vitorino, R. Domingues, F. Amado, P. Domingues, Oxidation of bovine serum albumin: identification of oxidation products and structural modifications, Rapid Commun. Mass Spectrom. 23 (2009) 2307–2315.
[93] G.V. Bochi, V.D. Torbitz, R.C. Santos, M. Cubillos-Rojas, J.L. López, A.M. Siebel, P. Gomes, J.R. de Oliveira, R.N. Moresco, Fenton reaction-generated advanced

oxidation protein products induces inflammation in human embryonic kidney cells, Inflammation 39 (4) (2016) 1285–1290.
[94] B. Tokur, K. Korkmaz, The effects of Fenton type (Fe^{+2}/H_2O_2) oxidation system on lipid and protein oxidation of grey mullet (Mugil cephalus), J. Fishscicom. 1 (1) (2007) 41–47.
[95] C.E. Grey, P. Adlercreutz, Evaluation of multiple oxidation products for monitoring effects of antioxidants in Fenton oxidation of 2'-deoxyguanosine, J. Argic. Chem. 54 (6) (2006) 2350–2358.
[96] C.P. Baron, L. Berner, L.H. Skibsted, H.H.F. Refsgaard, Evaluation of activity of selected antioxidants on proteins in solution and in emulsions, Free Radic. Res. 39 (7) (2005) 777–785.
[97] D. Zhang, H. Li, A.M. Emara, Y. Hu, Z. Wang, M. Wang, Z. He, Effect of in vitro oxidation on the water retention mechanism of myofibrillar proteins gel from pork muscles, Food Chem. 315 (2020), 126226.
[98] V. Chobot, F. Hadacek, G. Bachmann, W. Weckwerth, L. Kubicova, In vitro evaluation of pro- and antioxidant effects of flavonoid tricetin in comparison to myricetin, Molecules 25 (24) (2020) 5850.
[99] A.M. Fleming, J.G. Muller, I. Ji, C.J. Burrows, Characterization of 2′-deoxyguanosine oxidation products observed in the Fenton-like system Cu(II)/H_2O_2/reductant in nucleoside and oligodeoxynucleotide contexts, Org. Biomol. Chem. 9 (9) (2011) 3338–3348.
[100] I.M. Olivares-Corichi, G. Ceballos, R. Medina-Santillan, R. Medina-Navarro, A. M. Guzman-Grenfell, J.J. Hicks, Oxidation by reactive oxygen species (ROS) alters the structure of human insulin and decreases the insulin-dependent D-glucose-C14 utilization by human adipose tissue, Front. Biosci. 10 (2005) 3127–3131.
[101] T.L. Fink, P.J. Klepcyk, S.M. Oette, C.R. Gedeon, S.L. Hyatt, T.H. Kowalczyk, R. C. Moen, M.J. Cooper, Plasmid size up to 20 kbp does not limit effective in vivo lung gene transfer using compacted DNA nanoparticles, Gene Therapy 13 (13) (2006) 1048–1051.
[102] J. Louten, Essential Human Virology, Academic Press, 2016.
[103] X. Yang, Z. Yang, Z. Wu, Y. He, C. Shan, P. Chai, C. Ma, M. Tian, J. Teng, D. Jin, W. Yan, P. Das, J. Qu, X. p., Mitochondrial dynamics quantitatively revealed by STED nanoscopy with an enhanced squaraine variant probe, Nat. Commun. 211 (1) (2020) 3699.
[104] H. Ren, Y. He, J. Liang, Z. Cheng, M. Zhang, Y. Zhu, C. Hong, J. Qin, X. Xu, W. j., Role of liposome size, surface charge, and PEGylation on rheumatoid arthritis targeting therapy, ACS Appl, Mater. Interfaces 11 (22) (2019) 20304–20315.
[105] D.R. Witte, M.R. Taskinen, H. Perttunen-Nio, A. Van Tol, S. Livingstone, H. M. Colhoun, Study of agreement between LDL size as measured by nuclear magnetic resonance and gradient gel electrophoresis, J. Lipid Res. 45 (6) (2004) 1069–1076.
[106] H.P. Erickson, Size and shape of protein molecules at the nanometer level determined by sedimentation, gel filtration, and electron microscopy, Biol. Proced. Online 15 (11) (2009) 32–51.
[107] A.S. Olson, A.J. Jameson, S.K. Kyasa, B.W. Evans, P.H. Dussault, Reductive cleavage of organic peroxides by iron salts and thiols, ACS Omega 3 (10) (2018) 14054–14063.
[108] D. Balasubramanian, R. Kanwar, Molecular pathology of dityrosine cross-links in proteins: structural and functional analysis of four proteins, Mol. Cell Biochem. 234–235 (1–2) (2002) 27–38.
[109] J.W. Heinecke, W. Li, H.L. Daehnke 3rd, J.A. Goldstein, Dityrosine, a specific marker of oxidation, is synthesized by the myeloperoxidase-hydrogen peroxide system of human neutrophils and macrophages, J. Biol. Chem. 268 (6) (1993) 4069–4077.
[110] M. Moinpour, N.K. Barker, L.E. Guzman, J.C. Jewett, P.R. Langlais, J.C. Schwartz, Discriminating changes in protein structure using tyrosine conjugation, Protein Sci. 29 (8) (2020) 1784–1793.
[111] C. Cladaras, M. Hadzopoulou-Cladaras, R.T. Nolte, D. Atkinson, V.I. Zannis, The complete sequence and structural analysis of human apolipoprotein B-100: relationship between apoB-100 and apoB-48 forms, EMBO J. 5 (13) (1986) 3495–3507.
[112] J.W. Finley, Introduction: White papers from the "First International Congress on Antioxidant Methods", J. Agric. Food Chem. 53 (2005) 4288–4289.
[113] K.M. Schaich, X. Tian, J. Xie, Hurdles and pitfalls in measuring antioxidant efficacy: A critical evaluation of ABTS, DPPH, and ORAC assays, J. Funct. Foods 14 (2015) 111–125.